Mechanical Systems and Signal Processing 195 (2023) 110296

Contents lists available at ScienceDirect

Mechanical Systems and Signal Processing

journal homepage: www.elsevier.com/locate/ymssp

# Data-driven structural identification of nonlinear assemblies: Structures with bolted joints

S. Safari *, J.M. Londoño Monsalve

*Faculty of Environment, Science and Economy (ESE), University of Exeter, Exeter EX4 4QF, UK*

ARTICLE INFO

Communicated by Simon Laflamme

*Keywords:*
Nonlinear system identification
Virtual sensing
Bolted structures
Nonlinear damping
Reduced-order modelling
Model selection

ABSTRACT

The identification of nonlinearities that have a significant impact on dynamic behaviour of complex mechanical structures is necessary for ensuring structural efficiency and safety. A new methodology for structural identification of nonlinear assemblies is proposed in this paper that enables the discovery of stiffness and damping nonlinear models especially when it is not possible to directly measure the degrees of freedom where non-trivial nonlinearities are located. Input-output time-domain data collected at accessible locations on the structure are used to learn nonlinear models in the unmeasured locations. This is accomplished by making use of virtual sensing and model reduction schemes along with a physics-informed identification method recently developed by the authors (Safari and Londoño 2021). The methodology is suited for weakly nonlinear systems with localised nonlinearities for which their location is assumed to be known. It also takes into account dominant modal couplings within the identification process. The proposed methodology is demonstrated on a case study of a nonlinear structure with a frictional bolted joint, in numerical and experimental settings. It is shown that the model selection and parameter estimation for weakly nonlinear elements can be carried out successfully based on a reduced-order model which includes only a modal equation along with relevant modal contributions. Using the identified localised nonlinear models, both the reduced and full-order models can be updated to simulate the dynamical responses of the structure. Results suggests that the identified nonlinear model, albeit simple, generalises well in terms of being able to estimate the structural responses around modes which were not used during the identification process. The identified model is also interpretable in the sense that it is physically meaningful since the model is discovered from a predefined library featuring different nonlinear characteristics.

## 1. Introduction

Technologies that facilitate the accurate modelling of structures exhibiting nonlinear dynamical behaviour are becoming

*Abbreviations:* NSI, Nonlinear System Identification; FRF, Frequency Response Function; RSF, Restoring Force Surface; DOF, Degree of Freedom; SEREP, System Equivalent Reduction Expansion Process; IIRS, Iterative Improved Reduced System; PJSB, Principal Joint Strain Basis; POD, Proper Orthogonal Decomposition; FEM, Finite Element Model; SEEM, System Equivalent Model Mixing; FROLS, Forward Regression Orthogonal Least Square; NARMAX, Nonlinear Autoregressive Moving Average with eXogenous inputs; PNLSS, Polynomial Nonlinear State-Space; SINDy, Sparse Identification of Nonlinear Dynamics; CINDy, Conditional gradient-based Identification of Nonlinear Dynamics; NN, Neural Network; NNM, Nonlinear Normal Mode; MAC, Modal Assurance Criteria; ROM, Reduced Order Model.

* Corresponding author.
*E-mail address:* ss1072@exeter.ac.uk (S. Safari).

https://doi.org/10.1016/j.ymssp.2023.110296
Received 22 August 2022; Received in revised form 11 February 2023; Accepted 14 March 2023
Available online 22 March 2023

**Nomenclature**

| | |
|---|---|
| $i$ | Counter |
| $n$ | Number of time samples |
| $m$ | Number of degrees of freedom (DOFs) |
| $t$ | Time in *sec* |
| $\ddot{\boldsymbol{q}}$ | Acceleration vector of full-order model in the physical domain ($m/sec^2$) |
| $\dot{\boldsymbol{q}}$ | Velocity vector of full-order model in the physical domain ($m/sec$) |
| $\boldsymbol{q}$ | Displacement vector of full-order model in the physical domain ($m$) |
| $\boldsymbol{M}$ | Full-order mass matrix in physical domain |
| $\boldsymbol{C}$ | Full-order damping matrix in physical domain |
| $\boldsymbol{K}$ | Full-order stiffness matrix in physical domain |
| $\boldsymbol{F}$ | Excitation force on full-order model in the physical domain ($N$) |
| $f_{nl}$ | Nonlinear force ($N$) |
| $\boldsymbol{\rho}$ | Nonlinear element's location |
| $r$ | Number of nonlinear elements |
| $T$ | Transpose superscript |
| $\boldsymbol{q}_s$ | Slave degrees of freedom |
| $\boldsymbol{q}_m$ | Master degrees of freedom |
| $\boldsymbol{T}_G$ | Guyan transformation matrix |
| $\boldsymbol{T}_{IIRS}$ | IIRS transformation matrix |
| $\boldsymbol{M}_{IIRS}$ | Reduced mass matrix in physical domain |
| $\boldsymbol{K}_{IIRS}$ | Reduced stiffness matrix in physical domain |
| $\boldsymbol{C}_{IIRS}$ | Reduced damping matrix in physical domain |
| $F_{IIRS}$ | Excitation force on reduced-order model in the physical domain ($N$) |
| $\boldsymbol{K}_{ss}$ | Stiffness matrix of slave DOFs |
| $\boldsymbol{S}$ | Inverse of slave nodes' stiffness matrix |
| $\ddot{\boldsymbol{x}}$ | Acceleration vector of reduced-order model in the physical domain ($m/sec^2$) |
| $\dot{\boldsymbol{x}}$ | Velocity vector of reduced-order model in the physical domain ($m/sec$) |
| $\boldsymbol{x}$ | Displacement vector of reduced-order model in the physical domain ($m$) |
| $\boldsymbol{x^u}$ | Displacement vector of the unmeasured DOFs |
| $\boldsymbol{x^m}$ | Displacement vector of the measured DOFs |
| $\Phi_f$ | Matrix of linear, mass-normalized mode shapes of full-order model |
| $\Phi$ | Matrix of linear, mass-normalized mode shapes of reduced model in physical space |
| $\Phi^{\boldsymbol{u}}$ | Matrix of linear, mass-normalized mode shapes of the unmeasured DOFs |
| $\Phi^{\boldsymbol{m}}$ | Matrix of linear, mass-normalized mode shapes of the measured DOFs |
| $(\Phi^m)^\dagger$ | Left pseudo-inverse of matrix $\Phi^{\boldsymbol{m}}$ |
| $f_{nk}$ | Natural frequency of $k^{th}$ fundamental mode in ($Hz$) |
| $\omega_{nk}$ | Natural frequency of $k^{th}$ fundamental mode in ($rad$) |
| $\xi_k$ | Damping ratio of $k^{th}$ fundamental mode |
| $\boldsymbol{\varphi}_k$ | Mode shape vector of $k^{th}$ fundamental mode |
| $\boldsymbol{M}_s$ | Diagonal modal mass matrix |
| $\boldsymbol{C}_s$ | Diagonal modal damping matrix |
| $\boldsymbol{K}_s$ | Diagonal modal stiffness matrix |
| $\ddot{\boldsymbol{u}}$ | Modal acceleration response ($m/sec^2$) |
| $\dot{\boldsymbol{u}}$ | Modal velocity response ($m/sec$) |
| $\boldsymbol{u}$ | Modal displacement response ($m$) |
| $\boldsymbol{y}$ | Internal force vector |
| $\boldsymbol{y}^*$ | Input force vector |
| $n_c$ | Number of coupled modes |
| $\varepsilon_1, \varepsilon_2$ | Stopping criteria for model selection algorithm |
| $mm$ | Main mode |
| $mc$ | Coupled modes |
| $k_t$ | Iwan nonlinear model parameter (tangential stiffness) |
| $\beta$ | Iwan nonlinear model parameter (shape parameter) |
| $\chi$ | Iwan nonlinear model parameter (shape parameter) |
| $f_y$ | Iwan nonlinear model parameter (slip force) |
| $\sigma_g$ | Smooth transition parameter |
| $k_d$ | Contact stiffness in clearance model |

| | |
|---|---|
| $d$ | Clearance parameter (m) |
| $\varphi_{max}$ | Slip displacement |
| $c$ | Scaling constant |
| $\boldsymbol{p}$ | Vector of structural model parameters to be estimated |
| $\boldsymbol{p}_s$ | Vector of scaled structural model parameters |
| $MSE$ | Mean squared error |
| $\Delta MSE/\Delta s$ | Change of two consecutive MSE values |

increasingly important in engineering design and in digital twinning of civil, aerospace, automotive and naval structures. Nonlinear models that better predict the structure's amplitude of vibrations are best placed to ensure the structural safety when the structure is subjected to extreme operational conditions. Two main sources of nonlinearity in mechanical assemblies are geometric nonlinearity and local joints i.e., bolted joints. The sources of nonlinearities actively contributing to the response of the structural system need to be accurately identified using experimental measurements. Many Nonlinear System Identification (NSI) methods have been developed to detect, localise, characterise, and quantify nonlinearities directly from measurements in time and frequency domains [1–15]; they have been used to update and validate dynamic models of structures and assemblies. While detection step looks for deviations observed in a measured Frequency Response Function (FRF) based on expert judgement [16] and determine the statistical significance of the deviations [17], localisation step is realised by narrowing down to small number of possible locations based on engineering judgement [16] or intelligently using trained neural networks [18]. This paper focuses on automating two last steps i.e., characterisation and quantification which include the mathematical model selection (or form-finding) and parameter estimation for the selected model [13,16] respectively.

Characterisation and quantification typically involve solving optimisation problems. For example, Restoring Force Surface (RFS) method [19] using least squares approach in time domain and nonlinear parameter identification method via genetic algorithm optimisation in frequency domain [20]. An important limitation of these methods is the requirement of measurement from the nonlinear degree of freedom (DOF) as indicated by their authors as well. Attempts to overcome this limitation have been made based on neural networks trained using nonlinear frequency responses that help to locate the nonlinearity [18] and discover its type [17,18]. Training a neural network based on many scenarios of location and type (form) of nonlinearities in the system demands an intensive computational cost, although recent advances in reduced order modelling of nonlinear systems and computational methods for calculating nonlinear frequency responses seeks to alleviate the cost of this forward simulations [21–23]. Alternatively for structures with bolted joints, quasi static [24–30] and single nonlinear normal mode [10] techniques have been used to efficiently identify nonlinearities and update the numerical model while being limited for the cases that modal couplings are not present. In fact, most of the above cited NSI methods have at least one of the three following main drawbacks: (i) high computational effort, (ii) need to assume a nonlinear form (function) in the characterisation step which augments epistemic uncertainty, and (iii) ignore/disregard modal couplings throughout the identification process. To overcome the challenges, there is a growing interest in both academia and industry in developing data-driven structural identification tools able to identify low-dimensional parsimonious nonlinear structural dynamical models of complex mechanical systems. In data-driven methods, model reduction is carried out first, and then model selection methods are employed to identify the nonlinear dynamics in the reduced coordinates using regression techniques [31–33].

Regarding the reduced order modelling, the shared goal is the projection of the nonlinear response of the system onto a smaller number of DOF. Projection-based techniques reduce the model using modal basis either globally (Guyan static reduction [34], System Equivalent Reduction Expansion Process (SEREP) [35], Hurty/Craig Bampton method [36], Iterative Improved Reduced System (IIRS) [37]) or locally in which Principal Joint Strain Basis (PJSB) is used as an optimal local basis in [38] to reduce the size of the problem only in the joint locations. Locally reduced model is subsequently employed to identify a macro-model for the joints when the measurements are available in the joint vicinity and the couplings of the local modes are neglected [38]. Alternatively, there are approaches that carry out model reduction based on measured time-domain data (POD-Galerkin method [39], manifold learning techniques [40,41], autoencoders [42] or local basis approximation approach [22]).

Reduced order models derived using projection-based techniques when updated enable virtual sensing which combines the information in vibration measurements with the information in the Finite Element Model (FEM) of the structure. This feature is particularly helpful to expand the responses from measured to unmeasured locations and update the models of local joints existing in the FEM. Recently developed frequency-based sub-structuring approaches such as System Equivalent Model Mixing (SEMM) [43] are useful extensions to SEREP [35] that allows for similar accuracy with almost half the number of required experimental measurement points. SEMM has been used for identifying the joint dynamics with linear behaviour [44], however, its application to identify nonlinear joints needs further research. Virtual sensing and reconstruction of the physical responses in the linear structures can be carried out using only a few modal bases using projection-based method. When applied to nonlinear structures, it demands a high number of modal bases to accurately approximate the responses of the large-scale structures with nonlinear modal couplings. Therefore, this method might lose accuracy and effectiveness [23]. To the best of the authors' knowledge, the application of virtual sensing has not been explicitly addressed in the context of nonlinear identification. Therefore, it is essential to understand how model reduction and virtual sensing can be used to identify nonlinear models of local nonlinearities and reconstruct physical responses in unmeasured locations. Nevertheless, it should be noted that it is not the aim of this work to perform a comprehensive comparison of reduction/expansion techniques.

To address the limitation of assuming nonlinear model form, several automated model selection algorithms have been developed previously, including the Forward Regression Orthogonal Least Square (FROLS) algorithm [43] which is used in NARMAX variants

[44], Polynomial Nonlinear State-Space (PNLSS) [10], Sparse Identification of Nonlinear Dynamics (SINDy) [45], and Conditional gradient-based Identification of Nonlinear Dynamics (CINDy) [46]. These model selection algorithms have been commonly applied for the problems with the linear-in-parameters nonlinear models. Although, there are attempts recently to include parameterised nonlinear-in-parameter models in the library of candidate models [47], the complex form of nonlinearities in the engineering structures requires physics-informed model selection algorithms to deal with nonlinear models that are not linear-in-parameters. Moreover, Neural Network (NN)-based methods have been recently proposed to extend models of linear systems to include nonlinear models [48] and also helps to learn and approximate the system's Nonlinear Normal Modes (NNMs) [42]. The NN-based techniques, in contrast to sparse identification ones i.e. FROLS, SINDy and CINDy, are defined by exceedingly large parametrizations which typically lack interpretability or generalisability [45]. Here we understand by interpretability how well the identified model is related to the physical nature of the structure, for example, frictional model for the joints or polynomial model for the geometric nonlinearities. By generalisability we refer to the ability of the identified model to predict the behaviour of the identified structure under different loading within the limits of identified operational levels.

Although, the use of reduced models to describe full system dynamics is not new, its application to formulate a data-driven nonlinear identification method that discovers models of nonlinearities has been rarely reported [32]. Recently, a new direct optimisation-based model selection method for systems with only stiffness localised nonlinearities has been introduced by the authors in [49]. The method explicitly takes into account modal couplings while selecting nonlinear models from a comprehensive library of nonlinear terms including nonlinear-in-parameter functions. On that account, the main contribution of this paper is scaling up the methodology proposed in [49] to be applicable for more complex structures with multiple local nonlinear joints. It allows for automated data-driven model discovery of both stiffness and damping nonlinearities directly using time domain measurement data with no need to solve forward simulation during identification process. A two-stage model reduction scheme is employed to formulate the identification problem that allows identifying nonlinearities in known but inaccessible-to-measure locations. In this case, the equations of motion are projected into the modal domain after a model reduction in the physical domain. Besides, a virtual sensing strategy is used based on modal expansion in order to relax the necessity of direct measurement in the location of active nonlinear element. The proposed methodology is physics-informed, as it automatically incorporates nonlinearities into the underlying linear equations of motion of the structural system, which are assumed to be known, i.e., identified via linear model updating. The application of the proposed approach is demonstrated on nonlinear assembly with mechanical bolted joints (localised nonlinearities) and on a real-life experimental setup.

The rest of the paper is organised in five sections. Details of the proposed methodology for structural identification of nonlinear assemblies are described in Section 2. Section 3 presents the results for a virtual experiment structure where response data are simulated numerically representing a test condition. Section 4 discusses the application of the proposed method on physical experiment case where responses are measured using equipment conventionally used in modal testing. Lastly, the conclusions and highlights for future research are summarised in Section 5.

## 2. Methodology for the structural identification of nonlinear assemblies

This section presents a methodology for characterising and quantifying localised nonlinearities present in the mechanical structures that the authors have been developing over the past couple of years. The proposed method automatically searches for the best stiffness as well as damping nonlinear models that can be included into the equations of motion of a mechanical system based on a measured dynamic response data set. Unlike precedent works [4,49,50], in the methodology below there is no need to directly measure the response of the structure at the location of the nonlinear elements.

Consider a multi-degree-of-freedom mechanical system of the form below in the physical domain,

$$\boldsymbol{M}\ddot{\boldsymbol{q}}(t)+\boldsymbol{C}\dot{\boldsymbol{q}}(t)+\boldsymbol{K}\boldsymbol{q}(t)+\sum_{i=1}^{r}\boldsymbol{\rho}_i^T f_{nli}(\boldsymbol{\rho}_i\boldsymbol{q}(t),\boldsymbol{\rho}_i\dot{\boldsymbol{q}}(t))=\boldsymbol{F}(t) \tag{1}$$

where $\boldsymbol{M}$, $\boldsymbol{C}$ and $\boldsymbol{K}$ are the $m \times m$ matrices of mass, damping and stiffness, $\boldsymbol{F}$ is the force vector, $\boldsymbol{q}$, $\dot{\boldsymbol{q}}$, and $\ddot{\boldsymbol{q}}$ are, accordingly, the displacement, velocity and displacement $m \times n$ vectors. Here $m$ is the number of Degrees of Freedom (DOF) and $n$ is the number of time-domain samples. The nonlinear force vector $f_{nl}$ contains all conservative and non-conservative forces, and $\boldsymbol{\rho}$ is a location vector of the $r$ nonlinear elements. In order to keep the equations short, the time instance $t$ is omitted in the later equations.

The methodology starts with identifying and validating characteristics of underlying linear system i.e. natural frequencies ($f_{nk}$), damping ratios ($\xi_k$) and mode shapes ($\Phi_f$) using one of the standard available methods e.g. Polymax [51]. The identified characteristics are then used to update the linear FE model of the structure and build the updated mass, stiffness and damping matrices. The dynamic characteristics of updated underlying linear system are compared to the experimentally identified natural frequencies and mode shapes for validation. Modal assurance criteria (MAC) based on mode shapes higher than 0.95 and error of natural frequencies less than 1 percent are considered acceptable. Here, it is assumed that the location of nonlinear elements or the features introducing nonlinear behaviour are known, which is in most practical cases doable as it corresponds to joints, links, or other structural features. For nonlinear identification, a two-stage model reduction scheme is firstly introduced (Section 2.1) which facilitates the manipulation of large dynamical models (FE models) and reduces the dimension for both the simulation and identification problems. Secondly, a physics-informed nonlinear model selection and updating tool is employed for the characterisation and quantification of the localised nonlinearities existing in the structural system. In the last step, the identified nonlinear model is validated against the measured experimental data, i.e., time-domain responses or nonlinear frequency response curves. Fig. 1 summarises the methodology proposed in this paper for structural identification of nonlinear assemblies. It should be noted that the experiment design parts in flowchart refer

to selecting sensors and actuators locations as well as input excitation type. The following subsections provides detailed information about different part of the proposed methodology.

### 2.1. Model reduction and virtual sensing methodology

This section answers the question, how can we identify a nonlinear model if the response of the nonlinear element cannot be measured directly? To address this question, virtual sensing methodology after model reduction is employed and integrated into the proposed structural identification methodology.

In the first step, a model reduction in the physical domain is formulated in such a way that we group the degrees of freedom that are included in the measurement together with the degrees of freedom where the nonlinearity is located as master DOFs and group the remaining degrees of freedom as slave DOFs. For instance, in bolted structures the joint degrees of freedom would be included in the master DOFs group.

The IIRS method [37] is employed for model reduction in the physical domain which is highly accurate for linear systems. This method is selected due to its simple implementation, nevertheless, there are alternatives that could be used within the proposed identification method, e.g., Hurty/Craig Bampton method [36] and the local reduction using PJSB [38] if the couplings of the local modes are not neglected. We notice that this linear-based model reduction is appropriate for weakly nonlinear systems [10,52], which is the case for structures with bolted joints. Thus, the state transformation is considered in the form,

$$\begin{Bmatrix} \boldsymbol{q}_s \\ \boldsymbol{q}_m \end{Bmatrix} = \boldsymbol{T}_{IIRS}\{\boldsymbol{q}_m\} \tag{2}$$

where $\boldsymbol{T}_{IIRS}$ is the transformation matrix used to transfer the full-order model matrices to the Reduced-Order Model (ROM), $\boldsymbol{q}_m$ and $\boldsymbol{q}_s$ are respectively the responses from master and slave degrees of freedom. The IIRS method starts with deriving a transformation matrix $\boldsymbol{T}_G$ using Guyan reduction [34]. Static or Guyan reduction [34] is widely used to reduce the number of degrees of freedom in a finite element model but it is accurate only at zero frequency. Therefore, an iterative equation (Eq. (3)) is employed, which incorporates inertia terms into the reduction process to produce more accurate estimation of the full system's response, to calculate the improved transformation matrix $T_{IIRS}$.

$$\boldsymbol{T}_{IIRS,i+1} = \boldsymbol{T}_G + \boldsymbol{SMT}_{IIRS,i}\boldsymbol{M}^{-1}_{IIRS,i}\boldsymbol{K}_{IIRS,i} \tag{3}$$

where $\boldsymbol{M}_{IIRS,i}$ and $\boldsymbol{K}_{IIRS,i}$ are respectively reduced mass and stiffness matrices which can be calculated in each iteration as follows

$$\boldsymbol{M}_{IIRS,i} = \boldsymbol{T}^T{}_{IIRS,i}\boldsymbol{M}\boldsymbol{T}_{IIRS,i}, \boldsymbol{K}_{IIRS,i} = \boldsymbol{T}^T{}_{IIRS,i}\boldsymbol{K}\boldsymbol{T}_{IIRS,i} \tag{4}$$

where superscript $T$ indicates the transpose matrix. Iterations must be carried out for Eq. (3) until the eigenvalues and eigenvectors of the ROM match those of the full-order model up to a certain degree of accuracy. It is considered here that convergence is acceptable at 1% difference. It is important to include all relevant modes in the reduced basis set when building the reduced order model, otherwise the nonlinear ROM will not be adequate for its intended purpose. The addition of nonlinearity into the full order model essentially

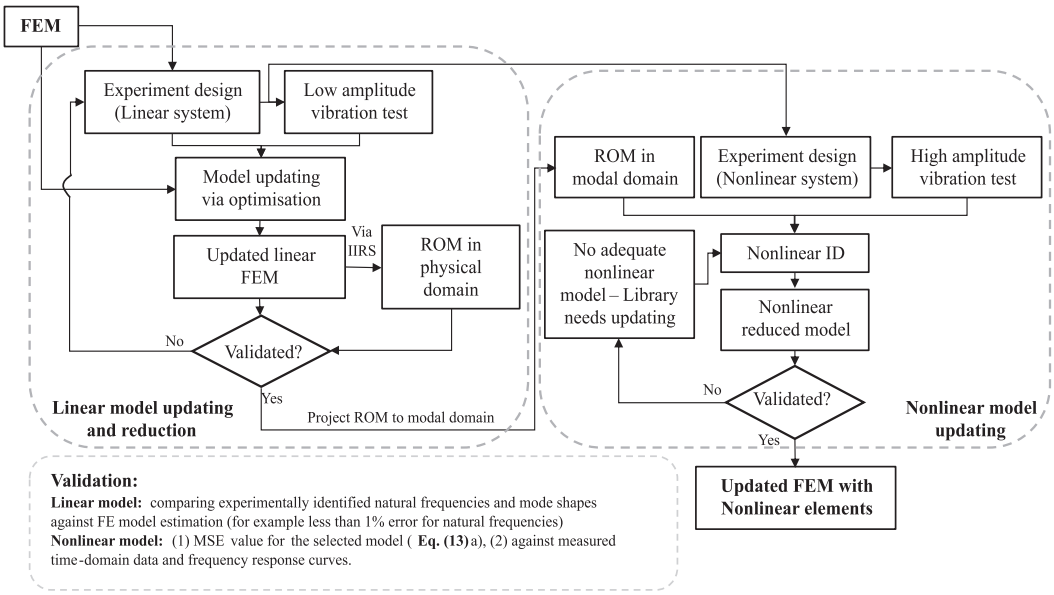


**Fig. 1.** Flowchart of the proposed methodology for the structural identification of nonlinear assemblies.

couples the underlying linear modes of the structure, so additional modes outside the typical bandwidth of interest considered for linear systems may be needed to account for such interactions [32]. Since weakly nonlinear structures are considered in this study, modes up to the 7th harmonic of the periodic input frequency are included. At each iteration, the reduced model will become more accurate. The speed of convergence depends on the choice of master degrees of freedom and a poor choice will lead to a very slow rate of convergence. In this paper, master DOFs include the nodes of nonlinear elements which are already known and the measurement points for which a number of low frequency modes is observable. Therefore, appropriate selection of measurement points leads to an ROM with a good approximation in the frequency range of the that modes [37]. The process of choosing master DOFs is carried out in the experiment design step for linear system which is indicated in Fig. 1. Here $S$ is calculated based on the stiffness matrix of slave DOFs as follows

$$\boldsymbol{S} = \begin{bmatrix} 0 & 0 \\ 0 & \boldsymbol{K}_{ss}^{-1} \end{bmatrix} \tag{5}$$

The transformation matrix ($\boldsymbol{T}_{IIRS}$) can be directly used in the Eq. (1) for model reduction by replacing $\boldsymbol{q} = \boldsymbol{T}_{IIRS}\boldsymbol{x}$ as follows

$$\boldsymbol{M}_{IIRS}\ddot{\boldsymbol{x}} + \boldsymbol{C}_{IIRS}\dot{\boldsymbol{x}} + \boldsymbol{K}_{IIRS}\boldsymbol{x} + \sum_{i=1}^{r} \boldsymbol{T}_{IIRS}{}^{T}\boldsymbol{\rho}_i^T f_{nli}(\boldsymbol{\rho}_i\boldsymbol{T}_{IIRS}\boldsymbol{x}, \boldsymbol{\rho}_i\boldsymbol{T}_{IIRS}\dot{\boldsymbol{x}}) = \boldsymbol{F}_{IIRS} \tag{6}$$

where the reduced mass and stiffness matrices are calculated according to Eqs. (4) and the external force is projected based on $\boldsymbol{F}_{IIRS} = \boldsymbol{T}_{IIRS}{}^{T}\boldsymbol{F}$. It should be noted that $\boldsymbol{x}$ is used here as the state variable for the reduced model in the physical domain instead of $\boldsymbol{q}_m$ in Eq. (2). The damping matrix $\boldsymbol{C}$ was formed using the matrix of underlying linear modal damping ratios $\xi_k$ according to equation below.

$$\boldsymbol{C} = \boldsymbol{M}\Phi_f \mathrm{diag}[2\omega_{nk}\xi_k]\Phi_f{}^{T}\boldsymbol{M} \tag{7}$$

where $\Phi_f$ is the matrix of linear, mass-normalized mode shapes $\boldsymbol{\varphi}_{fk}$, from the eigenvector problem,

$$\left(\boldsymbol{K} - \omega_{nk}^2\boldsymbol{M}\right)\boldsymbol{\varphi}_{fk} = 0. \tag{8}$$

Here, $\boldsymbol{K}$ is the underlying linear stiffness and $\omega_{nk}$ are linear natural frequencies where $k$ is the mode number. The reduced damping matrix $\boldsymbol{C}_{IIRS}$ is also derived similar to the reduced mass and stiffness matrices. The advantage of using a reduced-order model in the physical domain is that it keeps the measured and nonlinear-related DOFs in the model while preserving the dynamic properties of the underlying linear full-order model [23,37]. This is particularly of interest since the local nonlinear elements can be added to a linear model with low dimension in the physical domain which speeds up the numerical simulations.

Once model reduction in the physical domain has been done, the reduced-order model in Eq. (6) is projected into the modal domain using the matrix of linear mode shapes $\boldsymbol{x} = \Phi\boldsymbol{u}$ which results in Eq. (9). Here, $\Phi$ is the matrix of linear, mass-normalized mode shapes of the reduced order model in the physical domain. Thus, system dynamics can be expressed in terms of the linear modal coordinates $\boldsymbol{u}$.

$$\boldsymbol{M}_s\ddot{\boldsymbol{u}} + \boldsymbol{C}_s\dot{\boldsymbol{u}} + \boldsymbol{K}_s\boldsymbol{u} + \sum_{i=1}^{r} \Phi^T\boldsymbol{T}_{IIRS}{}^{T}\boldsymbol{\rho}_i^T f_{nli}(\boldsymbol{\rho}_i\boldsymbol{T}_{IIRS}\Phi\boldsymbol{u}, \boldsymbol{\rho}_i\boldsymbol{T}_{IIRS}\Phi\dot{\boldsymbol{u}}) = \Phi^T\boldsymbol{F}_{IIRS} \tag{9}$$

where $\boldsymbol{M}_s = \Phi^T\boldsymbol{M}_{IIRS}\Phi$, $\boldsymbol{C}_s = \Phi^T\boldsymbol{C}_{IIRS}\Phi$, and $\boldsymbol{K}_s = \Phi^T\boldsymbol{K}_{IIRS}\Phi$ are the diagonal modal matrices for mass, damping and stiffness. Diagonal modal matrices indicate decoupling of the equations of motion in the linear part, however coupling among linear modes remain and are due to the presence of nonlinear terms in the summation in Eq. (9). There are several key assumptions made during the reduction process: (a) that the structures behave linearly under low vibration levels, (b) that linear damping is modelled using viscous proportional damping [16,30] and (c) that the nonlinearities' locations are known. Accordingly, the linear part of Eq. (9) can be written in the form of Eq. (10) in terms of linear natural frequencies $\omega_{nk}$ and damping ratios $\xi_k$ when the mode shape matrix is mass-normalised.

$$\ddot{\boldsymbol{u}}_k + 2\xi_k\omega_{nk}\dot{\boldsymbol{u}}_k + \omega_{nk}^2\boldsymbol{u}_k + \sum_{i=1}^{r} \Phi^T\boldsymbol{T}_{IIRS}{}^{T}\boldsymbol{\rho}_i^T f_{nli}(\boldsymbol{\rho}_i\boldsymbol{T}_{IIRS}\Phi\boldsymbol{u}, \boldsymbol{\rho}_i\boldsymbol{T}_{IIRS}\Phi\dot{\boldsymbol{u}}) = \boldsymbol{\varphi}_k{}^{T}\boldsymbol{F}_{IIRS} \tag{10}$$

It should be noted that not only the reduced-order models generated in this section can be used to generate fast digital twins, enabling quick structural performance assessment in the nonlinear regime but also the formulation above aids in identifying the nonlinear models of the local nonlinear elements, whose responses cannot be measured. This is accomplished using virtual sensing which is incorporated into the formulation and detailed below.

The displacement $\boldsymbol{x}$ in Eq. (6) is divide into two parts: $\boldsymbol{x}^m$, which is displacement at the instrumented (or measured) DOFs and $\boldsymbol{x}^u$, which is the displacement at the unmeasured DOFs. Similarly, the matrix of linear mode shapes $\Phi$ in Eq. (10) is partitioned into $\Phi^m$ and $\Phi^u$ as:

$$\Phi = \begin{bmatrix} \Phi^m \\ \Phi^u \end{bmatrix}. \tag{11}$$

To estimate the structural responses at an unmeasured degree of freedom (DOF) using the updated linear FEM and the measured response time histories, a modal expansion approach can be used. For this purpose, $\boldsymbol{u}$ in Eq. (10) can be estimated using $\boldsymbol{x}^m$ and $\Phi^m$; consequently, the response time histories at the unmeasured DOFs, $\boldsymbol{x}^u$, can be estimated as

$$x^u = \Phi^u(\Phi^m)^{\dagger}x^m \tag{12}$$

in which $(\Phi^m)^{\dagger}$ indicates the left pseudo-inverse of matrix $\Phi^m$.

Ultimately, it is evident from Eq. (10) that the modal responses $\boldsymbol{u}$ are projected into the location of each nonlinear element using the transformations: modal transformation $\Phi$, improved transformation matrix $\boldsymbol{T}_{IIRS}$, and binary location matrix $\boldsymbol{\rho}$. Either Eq. (9) or Eq. (10) can be used directly to discover the nonlinear model and estimate unknown parameters using an optimisation process as presented in the following sections.

### 2.2. Parameter estimation

An optimisation problem can be defined based on Eq. (9) or Eq. (10) to estimate the parameters of the underlying linear system as well as the nonlinear model in the form of nonlinear algebraic regression. This nonlinear algebraic regression was inspired by numerical solvers of dynamic equations of motion, such as the Newmark method [53], which minimises residuals of internal and external forces. The required data for parameter estimation are the input excitation and structural responses, i.e., acceleration, velocity, and displacement (see Section 2.5) which are assumed to be measured experimentally. In this study, we assume a general case where all the parameters in Eq. (9) including linear and nonlinear parts should be updated. The optimisation problem of interest is now specified by the following cost function which minimises Mean Square Error (MSE) of internal and external forces as follow:

$$Minimise: MSE = \frac{1}{n}\sum_{i=1}^{n}\left(y^{*}_{mm_i} - y_{mmi}\right)^2 + \frac{1}{n_c}\sum_{j=1}^{nc}\frac{1}{n}\sum_{i=1}^{n}\left(y^{*}_{cm(j)_i} - y_{cm(j)_i}\right)^2 \tag{13a}$$

$$\boldsymbol{y}^{*} = \boldsymbol{\varphi}^{T}\boldsymbol{T}_{IIRS}{}^{T}\boldsymbol{F} \tag{13b}$$

$$\boldsymbol{y} = \boldsymbol{M}_s\ddot{\boldsymbol{u}} + \boldsymbol{C}_s\dot{\boldsymbol{u}} + \boldsymbol{K}_s\boldsymbol{u} + \sum\nolimits_{i=1}^{r}\boldsymbol{\varphi}^{T}\boldsymbol{T}_{IIRS}{}^{T}\boldsymbol{\rho}_i^{T}f_{nli}(\boldsymbol{\rho}_i\boldsymbol{T}_{IIRS}\boldsymbol{\varphi}\boldsymbol{u}, \boldsymbol{\rho}_i\boldsymbol{T}_{IIRS}\boldsymbol{\varphi}\dot{\boldsymbol{u}}) \tag{13c}$$

where $n$ is the size of the time-series data; $\boldsymbol{y}^{*}$ and $\boldsymbol{y}$ are the input force and internal force vectors respectively. Subscripts $mm$ and $cm$ indicate the mode number for main and coupled modes, and $n_c$ is the number of coupled modes. The mode in which the structure is excited (close to a natural frequency) is chosen to be the main mode. Coupled modes are those in which a strong coupling to the main mode is anticipated. These modes can be selected by observing the energy of modal responses such as cumulative energy of time response.

Any nonlinear optimiser could be employed to solve the optimisation problem defined in Eq. (13a). Several optimisers have been assessed by the authors in [33] for the general nonlinear identification problem in Eq. (13) which the interested readers can refer to for more details. Based on those results, we use gradient based Levenberg-marquardt (LM) optimisation algorithm [54] with a multi-start strategy.

Three factors are essential for successfully running the nonlinear optimisation problem: scaling, initialisation and bounding for all parameters in the search space. The measured physical responses of the structure and also the information obtained from linear modal testing help to define a physics-informed space of search and to tailor the optimisation problem for identifying models of nonlinear mechanical structures. In this paper, a new bi-symmetric logarithmic scaling according to Eq. (14) is used to scale the search space of parameters which handles negative values while maintaining continuity across zero [55].

$$p_s = \text{sign}(p)(log_{10}(1 + \frac{|p|}{c})), \tag{14a}$$

$$p = \text{sign}(p_s)c(-1 + 10^{|p_s|}) \tag{14b}$$

Here, $c$ is a scaling constant which controls how much the search space is compressed/stretched and is set to 1 in this study, $p$ is the unscaled (true) parameter value and $p_s$ is the corresponding value in the scaled space. The employed scaling scheme is suitable for the multi-dimensional parameter spaces with different order of magnitudes. The bounds for the linear parameters are defined based on the variations of 5% of natural frequencies and 20% of linear damping ratios obtained from linear modal identification. A low variation for linear frequencies and high variation for damping ratios are considered. For nonlinear parameters sum of the maximum absolute linear force $f_{lmax}$ (inertia $\max(|\boldsymbol{M}\ddot{\boldsymbol{q}}|)$, damping $\max(|\boldsymbol{C}\dot{\boldsymbol{q}}|)$ and stiffness forces $\max(|\boldsymbol{K}\boldsymbol{q}|)$) divided by the maximum quantity of selected nonlinear term is used for bounding the parameters. For example, in the case that the nonlinear force is described by $f_{nl}(\boldsymbol{q}) = p(1)\boldsymbol{q}^3$, its parameter $p(1)$ is bounded with $\pm f_{lmax}/\max(|\boldsymbol{q}^3|)$. For considering higher variability in the parameters, it is possible to make the bounds wider by multiplying a coefficient higher than one. In addition, the maximum relative displacement/velocity in the location of nonlinear elements is used to define the bound of the parameters with displacement/velocity units in the nonlinear model.

The initialisation for linear parameters is done based on the identified values for natural frequencies and damping ratios from linear modal testing. The nonlinear model parameters are initialised randomly using multi-start strategy with 50 different values for each parameter within the specified bounds. Nonetheless, during the model selection estimated values for the parameters of a specific nonlinear term are recorded to be used in the following iteration of the model selection (see Section 2.3). It should be noted that the bounding and initialisation are also defined in the scaled space. Interested readers can refer to [33,49] for more details on defining a physics-informed space of search for the optimisation problem in the context of structural identification of nonlinear structures.

### 2.3. Model selection method

In this section, forward–backward (FB) model selection algorithm is described for discovering nonlinear models based on the

optimisation problem define in Section 2.2. The algorithm uses a predefined and comprehensive library of nonlinear terms typically encountered in common engineering structures (Section 2.4, Table 1). In general, the FB algorithm concerns the forward selection process of nonlinear terms from the library by adding them to the structural model one at a time. Forward selection has the advantage that it starts with the underlying linear model and uses the estimated parameters of last selected nonlinear model as initial conditions before adding a new term in the following stage. In a high dimensional search space, this reduces the possibility of getting trapped in local minima. Afterward, a backward elimination process is performed to eliminate terms with a negligible contribution and to provide a parsimonious model. The progressive initialisation of parameters is also considered here while removing the terms one by one. The important steps of FB algorithm are summarised below, and a full detail may be viewed in [49].

The steps for forward selection include:

1. Minimise MSE in Eq. a) considering one nonlinear term from Table 1 added to the nonlinear model ($f_{nl}$).
2. Repeat step 1 considering different nonlinear term from Table 1 added to the nonlinear model ($f_{nl}$), until all terms are individually added.
3. Select the nonlinear term that produced the minimum MSE value and keep it as part of the dynamic model in Eq. (9).
4. If stopping criteria are not met, go back to step 1 and add another nonlinear term; otherwise deliver the nonlinear dynamic model.

The steps for backward selection include:

1. Start with the nonlinear model transferred from latest step of forward selection.
2. Create a new nonlinear model by eliminating one nonlinear term and minimise the MSE in Eq. (13a).
3. Repeat step 2 by eliminating a different nonlinear term from the nonlinear model.
4. Once removing each nonlinear term has been examined, select the nonlinear model with the lowest MSE.
5. If stopping criteria are not met, go back to step 2 and remove another nonlinear term; otherwise deliver the nonlinear dynamic model.

Two stopping criteria, MSE value and $\Delta MSE/\Delta s$, are needed in the process of model selection. Here $s$ is the progression number of the model selection algorithm. Specifically, $MSE$ value is considered when its value drops lower than user-assigned threshold $\varepsilon_1$. Besides, when the change of two consecutive $MSE$ values ($\Delta MSE/\Delta s$) is less than $\varepsilon_2$, the algorithm stops and delivers the nonlinear

**Table 1**
Library of nonlinear terms used in this study.

Linear-in-parameters nonlinear terms

| Index | Term | Index | Term | Index | Term | Index | Term |
|---|---|---|---|---|---|---|---|
| 1 | $q\lvert q\rvert$ | 12 | $\lvert q\rvert q\dot{q}$ | 23 | $\lvert q\rvert\dot{q}$ | 34 | $\dot{q}^9$ |
| 2 | $q^3$ | 13 | $q^3\dot{q}$ | 24 | $\lvert q\rvert^{1.5}\dot{q}$ | 35 | $\sqrt{\lvert\dot{q}\rvert}$ |
| 3 | $\lvert q\rvert q^3$ | 14 | $\lvert q\rvert q^3\dot{q}$ | 25 | $\lvert q\rvert^2\dot{q}$ | 36 | $\lvert\dot{q}\rvert^2$ |
| 4 | $q^5$ | 15 | $q^5\dot{q}$ | 26 | $\mathrm{sign}(\dot{q})$ or $\dot{q}/\lvert\dot{q}\rvert$ | 37 | $\lvert\dot{q}\rvert^3$ |
| 5 | $\lvert q\rvert q^5$ | 16 | $\lvert q\rvert q^5\dot{q}$ | 27 | $\lvert\dot{q}\rvert\dot{q}$ | 38 | $\lvert\dot{q}\rvert^4$ |
| 6 | $q^7$ | 17 | $q^7\dot{q}$ | 28 | $\dot{q}^3$ | 39 | $\lvert\dot{q}\rvert^5$ |
| 7 | $\mathrm{sign}(q)\sqrt{\lvert q\rvert}$ | 18 | $\mathrm{sign}(q)\sqrt{\lvert q\rvert}\dot{q}$ | 29 | $\lvert\dot{q}\rvert\dot{q}^3$ | 40 | $\lvert\dot{q}\rvert^6$ |
| 8 | $q\sqrt{\lvert q\rvert}$ | 19 | $\sqrt{\lvert q\rvert}q\dot{q}$ | 30 | $\dot{q}^5$ | 41 | $\lvert\dot{q}\rvert^7$ |
| 9 | $q\lvert q\rvert\sqrt{\lvert q\rvert}$ | 20 | $\sqrt{\lvert q\rvert}q\lvert q\rvert\dot{q}$ | 31 | $\lvert\dot{q}\rvert\dot{q}^5$ | | |
| 10 | $q^3\sqrt{\lvert q\rvert}$ | 21 | $\sqrt{\lvert q\rvert}q^3\dot{q}$ | 32 | $\dot{q}^7$ | | |
| 11 | $q\dot{q}$ | 22 | $\sqrt{\lvert q\rvert}\dot{q}$ | 33 | $\lvert\dot{q}\rvert\dot{q}^7$ | | |

Nonlinear-in-parameters nonlinear terms

| Index | Term | Description |
|---|---|---|
| 42 | $\begin{cases} k_t q & \lvert k_t q\rvert < f_s \\ f_y \mathrm{sgn}(q) & \text{otherwise} \end{cases}$ | ***Jenkins model*** <br> $k_t$: *Tangential stiffness,* $f_y$*: Slip force* |
| 43 | $f_y((2/(1+e^{(-\sigma_g q)}))-1)+k_t q$ | ***Generalised Jenkins Prager model*** <br> $\sigma_g$*: smooth transition parameter* |
| 44 | $\begin{cases} \mathrm{sgn}(q)(k_d(\lvert q\rvert - d/2)) & \lvert q\rvert > d/2 \\ 0 & \text{otherwise} \end{cases}$ | ***Clearance model*** <br> $k_d$*: contact stiffness, d: clearance* |
| 45 | $\begin{cases} k_t q - \left(\left(\frac{k_t\left(\beta+\frac{\chi+1}{\chi+2}\right)}{f_y(1+\beta)}\right)^{1+\chi}\frac{k_t}{(1+\beta)(\chi+2)}\right)q^{\chi+2} & \lvert q\rvert < \varphi_{max} \\ f_y \mathrm{sgn}(q) & \lvert q\rvert \geq \varphi_{max} \end{cases}$ | ***4-parameter Iwan model*** <br> $\varphi_{max} = \frac{f_y(1+\beta)}{k_t(\beta+\frac{\chi+1}{\chi+2})}$ *and* $\chi$ *are the shape parameters.* |
| 46 | $\begin{cases} k_t q - \left(\left(\frac{k_t\left(\beta+\frac{\chi+1}{\chi+2}\right)}{f_y(1+\beta)}\right)^{1+\chi}\frac{k_t(\chi+1)}{(1+\beta)}\right)\left(\frac{\theta}{\chi+2}-\frac{1}{\chi+1}\right)q^{\chi+2} & q < \varphi_{max} \\ \theta f_y & q \geq \varphi_{max} \end{cases}$ | ***5-parameter Iwan model*** <br> $\theta$*: The ratio of slip force to force required to initiate slip* |

model. These rules are applied contrariwise when eliminating the nonlinear terms using backward regression. Notice that the latter criterion is determinant in the cases when by adding/removing more nonlinear terms, the model prediction does not improve significantly.

### 2.4. Library of nonlinear terms

One of the advantages of using a nonlinear optimisation algorithm for solving the identification problem as defined here in Eq. (13a) is that linear- and nonlinear-in-parameter functions can be deployed in the library of nonlinear terms. This provides a good flexibility and accuracy in deriving a parsimonious model for local nonlinearities in the system. In this paper, we consider both stiffness (displacement-dependent) and damping (displacement- and velocity-dependent) nonlinearities in the identification process since considering low order polynomials for real-life nonlinearities is only a coarse approximation [10]. The library used in this work includes polynomial, clearance, and frictional nonlinear model terms which are commonly employed in modelling structures with nonlinear joints [25]. It should be noted that including hysteresis type frictional models [11], which are normally rate dependent, needs special attention and are out of the scope of this study. However, this will be considered in the future extensions of this work. Table 1 shows the predefined library of nonlinear terms used in this study.

### 2.5. Testing and data processing

Due to the complex behaviour of nonlinear structures (e.g., amplitude-dependent properties, jumps, sub/super harmonics, modal interactions, etc), nonlinear dynamic testing demands more data and effort than linear testing. In this work, we are considering both harmonically forced and free decay responses in the time-domain as they provide useful information for nonlinear identification. Harmonic force (sweep-sine) excites the structure nearby the resonant frequency of a target mode for a particular response level. Excitation levels should be set based on the performance that is expected over the course of a structure's lifetime. Besides, free vibration response, when setting the system free after arriving at a desired response nearby a resonance, contains information about all of the underlying fundamental features of a dynamical system, including those properties that are susceptible to change as a function of the vibration amplitude. Therefore, the time series data recorded from forced and free decay responses nearby the fundamental natural frequencies of interest or, alternatively, data for a single sweep-sine test covering a specific frequency bandwidth can be collected. After that, the data belonging to a single or multiple fundamental natural frequency can be used for model identification.

Accelerometers are the typical response acquisition approach used in modal testing. Here we assume that an array of accelerometers is placed on the structure to measure its dynamic responses at multiple points. The time-domain data required for the proposed methodology here include acceleration, velocity, and displacement response records and also the applied excitation force. While acceleration and excitation forces are measured directly, displacement and velocity response data are obtained from experimentally measured acceleration data by numerical integration [7].

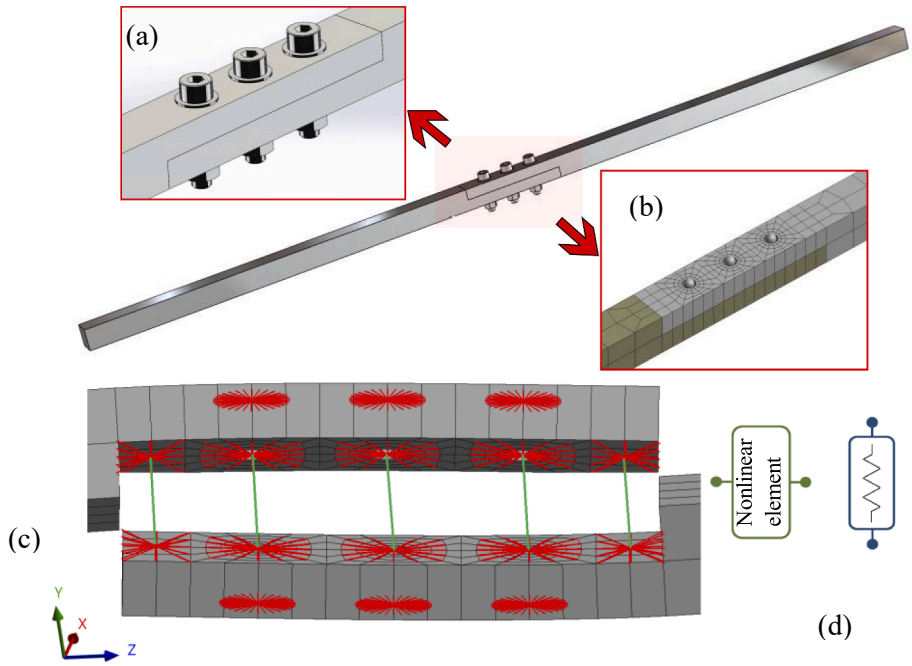


**Fig. 2.** Illustration of the Brake-Reuß beam (a) CAD model, (b) finite element mesh, and point mass, (c) joint configuration, and (d) whole joint model.

## 3. Virtual experiment

In this section, the proposed nonlinear model identification method is demonstrated by identifying mathematical models for localised nonlinearities of a nonlinear FE model. The model is described in Section 3.1. In order to study the accuracy of different model reduction orders 4 ROMs are introduced and studied in Section 3.2. In addition, the effects of modal couplings on the response prediction of the model in modal space is investigated based on the comparison of time series and amplitude dependent dynamic characteristics of the structure in Section 3.3. Finally, the proposed methodology is used to identify the nonlinear model of the structure under study.

### 3.1. Model description

We consider a length-modified Brake–Reuß beam (LBRB) [28] which is shown in Fig. 2(a). The LBRB consists of two beam components with square cross-section that are bolted through a three-bolted lap-joint together to form a long beam. The total length of the beam is about 1080 mm (42.5 in) and the cross-section of the beams is a 25.4 mm × 25.4 mm (1 in × 1 in) square. Three sets of M8 bolts, nuts and standard washers are used for the assembly, which has a 120 mm × 25.4 mm contacting interface. The exact dimensions and drawings of the structure can be found in [28].

A finite element model for the two components of the beam was built using higher-order hexahedron elements with 20 nodes that exhibit quadratic displacement behaviour. A linear-elastic, isotropic material model was used and the density, Young's modulus and Posson's ratio were assigned to be 7800 kg/m$^3$, 200 GPa, and 0.29 respectively. MultiZone meshing technique for different zones of the beam are used such that a denser mesh nearby the joint and a coarser mesh for the far ends of the beam (see the mesh zone change in Fig. 2(b)). This is different from the other studies [28–30] with uniform dense mesh for all parts.

Owing to its computational advantage, for modelling the bolted lap joint, we considered the "whole-joint" approach presented by Lacayo et al. [29]. In this modelling technique, the physical bolts are removed and replaced with point masses (See Fig. 2 (b)) at each side of the bolt hole. The bolt, washer, and nut set weighs 31.34 g. As depicted in Fig. 2(c), the interface is divided into five patches for each part of the beam: three of equal area surrounding each bolt hole, and two of a smaller area on each end of the interface. The displacements and rotations of each of these patches is coupled to a virtual node with six DOFs. A set of multi-point constraints (MPCs) are formulated to set each DOF of the virtual node to the average of the nodes in its corresponding patch. The virtual nodes associated with two opposing contact patches were then connected to each end of a "whole-joint model". For each patch, the whole-joint model is characterised by a linear spring in the normal direction to the patch and a nonlinear element in the tangential direction to the patch according to Fig. 2(d).

For this virtual experiment example, all five whole-joint models consists of a linear spring with stiffness $1 \times 10^8 Nm^{-1}$ connecting the normal (Y) direction DOF and a 4-parameter Iwan element (Table 1, No 39) with parameters $f_y = 2000N$, $k_t = 1 \times 10^8 Nm^{-1}$, $\chi = -0.5$, and $\beta = 0.1$ connecting the axial (Z) direction DOF. The linear spring represents the stiffness of the interface caused by the bolt pretension, and the Iwan element represents the friction associated with tangential motion near each joint.

The full-order finite element model consists of 12,492 DOFs. The full-order model is reduced using the IIRS method introduced in Section 2.1. It is worth noting that we assume the linear structural model to be known for this virtual experiment, but that in the case of a physical experiment, the underlying linear model would need to be updated (as discussed later in Section 4.2). Here, four different reduced-order models are created for the sake of comparison. The first model (named ROM1) includes 12 DOFs in (Y) direction which are kept in the model (representing measurement points - See Fig. 3) on top of the 20 (5 patches × 2 parts × 2 DOF) virtual joint nodes (representing the DOF where the nonlinear element is connected to) as master DOFs which are used to connect the two beam components. As it will be shown later, this model, which is able to explicitly embed nonlinear elements and DOFs in the physical domain, could be used as an alternative to the full-order model with negligible error. In the second model (ROM2), only 12 DOFs in (Y) direction are retained as master nodes where the effects of nonlinearities in the system are incorporated based on the transformation matrix introduced in Eq. (6). The third model (ROM3) describes the system in the modal domain according to the Eqs. (9) and (10). Since the identification problem is formulated based on ROM3, therefore, its accuracy in responses estimation is important. Another model (ROM4) is created based on ROM1 where all 32 DOF kept in the model and then reduced to the modal space. In ROM4, only the measured degrees of freedom are retained in the mode shape matrix in order to transfer the physically measured responses into modal

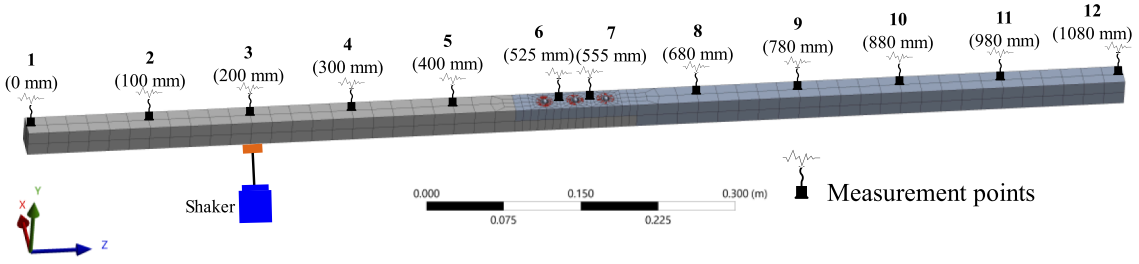


**Fig. 3.** Selected measurement points in the experiment structure.

responses. Afterward, all degrees of freedom in the mode shape matrix are used when setting the optimisation problem according to Eq. (13) to map the measured responses into the nonlinear joints appropriately.

The modal Assurance Criteria (MAC) and natural frequencies were calculated to compare ROM1 (derived using the IIRS method) against full-order FE model. Within 100 iterations of the IIRS procedure based on Eq. (3), the first 10 bending modes of the ROM1 match with those of the full-order model with less than 1 percent error. Fig. 4a shows the MAC for the first 10 bending modes. These present good results evidenced by the high MAC values in the diagonal. The first four bending linear modes shapes of the structure are also shown in Fig. 4b for the full-order and ROM1 derived using the IIRS method. It can be seen that the mode shapes estimated using the reduced-order model are in a good agreement with the full-order model.

In addition, the approximation error of natural frequencies of the first 10 bending mode between the FE model and the ROM1 are reported in Table 2. Since the approximation error is considerably low (the highest error is 0.24 percent in the mode 9), it can be justified that the ROM1 with only 32 DOFs can be used as an alternative to the full-order FE Model, within the respective frequency bandwidth (10–4400 Hz).

Before running the nonlinear time history simulations of the reduced-order FE models described above, the equations of motion in Eq. (6) undergoes another basis change to remove the rigid body modes. This basis change stems from the definition for constraining the rigid body modal coordinates,

$$\boldsymbol{\varphi}_R^T \boldsymbol{M}_{IIRS} \boldsymbol{x} = 0 \tag{15}$$

where $\boldsymbol{\varphi}_R$ is a set of the zero-energy mode shapes (mass-normalized) produced from Eq. (8). The non-trivial solutions to Eq. (15) lie in the null space of $\boldsymbol{\varphi}_R^T \boldsymbol{M}_{IIRS}$ and the set of all non-trivial solutions according to equation below,

$$\boldsymbol{L} = null(\Phi_R^T \boldsymbol{M}_{IIRS}), \tag{16}$$

forms the Ritz basis matrix $\boldsymbol{L}$ that is used to transform Eq. (6) by substituting $z = \boldsymbol{L}\boldsymbol{x}$ and premultiplying by $\boldsymbol{L}^T$ yields the final system equations of motion,

$$\boldsymbol{M}_L z + \boldsymbol{C}_L \dot{z} + \boldsymbol{K}_L z + \sum_{i=1}^{r} \boldsymbol{L}^T \boldsymbol{T}_{IIRS}{}^T \boldsymbol{\rho}_i^T f_{nli}(\boldsymbol{\rho}_i \boldsymbol{T}_{IIRS} \boldsymbol{L} z, \boldsymbol{\rho}_i \boldsymbol{T}_{IIRS} \boldsymbol{L} \dot{z}) = \boldsymbol{F}_L. \tag{17}$$

In Eq. (17), $\boldsymbol{M}_L$, $\boldsymbol{C}_L$, $\boldsymbol{K}_L$, and $\boldsymbol{F}_L$ are derived as follow,

$$\boldsymbol{M}_L = \boldsymbol{L}^T \boldsymbol{M}_{IIRS} \boldsymbol{L}, \boldsymbol{C}_L = \boldsymbol{L}^T \boldsymbol{C}_{IIRS} \boldsymbol{L}, \boldsymbol{K}_L = \boldsymbol{L}^T \boldsymbol{K}_{IIRS} \boldsymbol{L}, \boldsymbol{F}_L = \boldsymbol{L}^T \boldsymbol{F}_{IIRS} \boldsymbol{L}. \tag{18}$$

Now, Eq. (17) can be solved in the time domain to obtain the nonlinear dynamic responses.

### 3.2. Simulation responses of reduced models

Here, we run nonlinear time history simulations for the reduced-order models described above to assess their accuracy. Responses are compared in terms of two amplitude-dependent properties: the instantaneous frequency and damping, which are obtained from transient free-response simulations using the zero-crossing method introduced by Londoño et al. [5]. In this method the structure is vibrated at the desired resonance condition, the forcing is removed, and the resulting resonance decay vibration response analysed using zero crossing method to estimate the instantaneous frequency and amplitude of oscillations. For each simulation, equations of motion were integrated using Hilber-Hughes-Taylor-α (HHT-α) [56] which is a generalization of the Newmark-β method and allows for

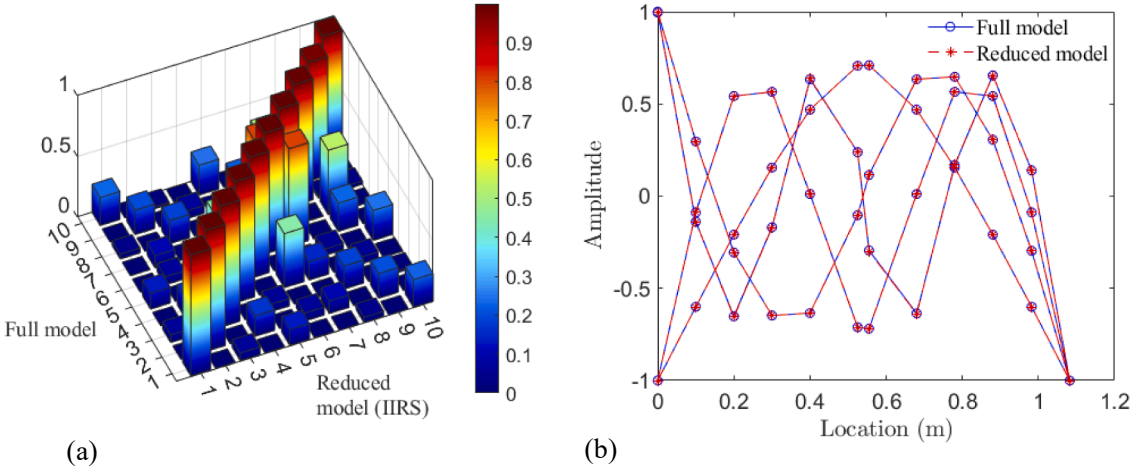


**Fig. 4.** Comparison of the underlying linear system for full-order model and ROM1 (a) MAC diagram, and (b) first four bending linear modes shapes.

**Table 2**
Fundamental frequencies of underlying linear system and error of reduced-order model (ROM1) in the physical domain with respect to the full-order FE model.

| Bending mode | 1 | 2 | 3 | 4 | 5 | 6 | 7 | 8 | 9 | 10 |
|---|---|---|---|---|---|---|---|---|---|---|
| $f_n$ (Hz) | 78.56 | 288.84 | 515.3 | 837.91 | 1329.66 | 1481.95 | 1938.58 | 2509.94 | 2929.71 | 4383.22 |
| Error (%) | 0.002 | $1.5 \times 10^{-5}$ | $5.2 \times 10^{-5}$ | $1.5 \times 10^{-6}$ | $1.9 \times 10^{-5}$ | $9.2 \times 10^{-5}$ | −0.0007 | 0.007 | 0.24 | 0.03 |

numerical energy dissipation and second order accuracy.

To compare the reduced-order models, the simulations are initialized from a deformed shape corresponding to the first bending mode, with amplitude of 4 mm at the tip of beam (point 12 in Fig. 3). Fig. 5 shows the response of the tip of the beam with five nonlinear joint elements. The comparison of the responses for ROM2 and ROM3 against ROM1, which we here considered as an alternative to full-order model, shows that the ROM2-3 models can predict the trend of amplitude-dependent instantaneous frequency and damping. Therefore, they can still be used for model discovery. The response for ROM3 (solid blue line), which includes only 12 measured degrees of freedom and one mode in the modal domain, provides evidence that the form of the nonlinearity can be discovered even when using only one modal equation of motion. The response generated from ROM4 (where the joint DOFs are also kept in the model and the reduction to the modal space is done with 12 modes) in black dashed line, shows that including higher modes and taking modal couplings into account in the equations of motion help in reproducing fairly accurate responses for the full model of weakly nonlinear systems.

When using reduced-order models for simulation or identification, computational time is a critical criterion. The simulation was conducted during the time interval of 80 s with sampling frequency equal to $F_s = 2^{13}$ Hz. Using the ROMs studied above, the computational time of a time history dynamic simulation is nearly 40 s, whereas the full-order model with 12,492 DOFs requires more than 55 min. All simulations have been run on a standard PC with six cores CPU and 16 GB of RAM.

### 3.3. Modal coupling effect on the parameter estimation

To demonstrate the positive effects of considering explicitly the modal couplings on the model identification and parameter estimation using the NSI method proposed here, the virtual structure is excited with a harmonic sweep sine force with amplitude 40 N and frequency sweeping back from 76.5 to 78 Hz at the point 3 (see Fig. 3). After achieving a resonant condition, the force is zeroed, and free decay responses are obtained. The recorded displacement response from point 12 is shown in Fig. 6a. Three parts of the response including initial transient, near resonance and decaying parts are selected as training data set (see Fig. 6a) to be used. The responses include acceleration, velocity and displacement form points 1–12.

Prior to the identification step, two cases are examined to show the application of the virtual sensing which helps to identify the model of the joints. The measured responses at 12 points are projected to the location of joints using (i) the mode shapes of the full order model and the binary location matrix $\boldsymbol{\rho}$, (ii) the transformations: modal transformation $\Phi$, improved transformation matrix $\boldsymbol{T}_{IIRS}$, and binary location matrix $\boldsymbol{\rho}$. For both cases 10 bending modes in the direction of excitation are used. The reconstructed nonlinear force–displacement responses at the location of an outer joint are compared with the force–displacement response of the true system joint in Fig. 6b. It can be seen that the two-stage transformation approach is reconstructing the force–displacement response with better accuracy when discovering the nonlinear model for the joints.

In the identification process, the ROM4 is used based on three different scenarios outlined in Table 3. In these scenarios, modal equation of motion refers to Eq. (10) and it is important to select the main mode based the excitation frequency for the identification purpose according to Section 2.2. Modal coupling due to nonlinearity refers to the number of the mode shapes $\Phi$ used within the nonlinear part ($f_{nl}$) of the Eq. (10). When only one mode shape is used within the nonlinear part ($f_{nl}$) it means that no modal coupling is considered in the identification process. Notice that, as it was described in Section 2.5, the proposed data-driven identification method considers carrying out regression using acceleration (measured), velocity and displacement (from integration [7]) responses, and therefore, there is no need to solve the differential equation during the identification process. The modal equation of only one mode is used for identification within optimisation problem in Eq. (13a) including nonlinear part ($f_{nl}$) with multiple mode (S2 in Table 3). This phase can be considered as offline phase which is followed by online simulation phase for validation.

For the sake of completeness, we firstly assume that the nonlinear model is known, but that parameters need to be estimated for each of the abovementioned scenarios. The estimated parameters of the Iwan model are reported and compared with the true parameters in Table 4.

The nonlinear model for each patch in the joint is considered to have the same form (same physics) but with a different set of parameters. From Table 4 it can be observed that the estimated parameters for the outer patches (elements 1 and 5) are within a similar range. The same observation can be made for the inner patches (elements 2 and 4). This is consistent with the structure's symmetric

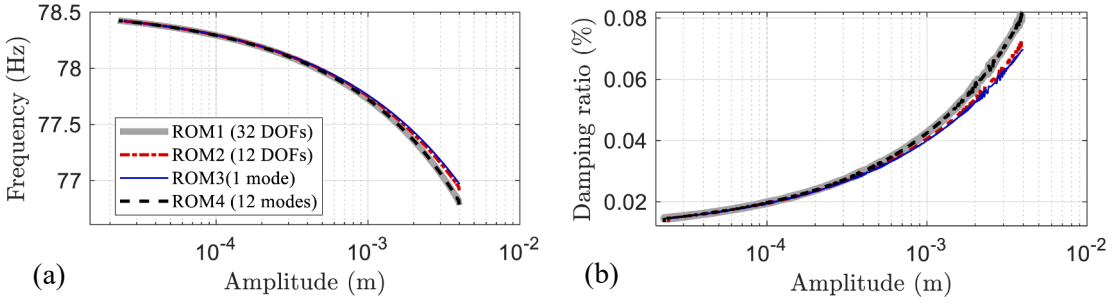


**Fig. 5.** Amplitude dependent response of beam tip (point 12) (a) instantaneous frequency, and (b) instantaneous damping ratio.

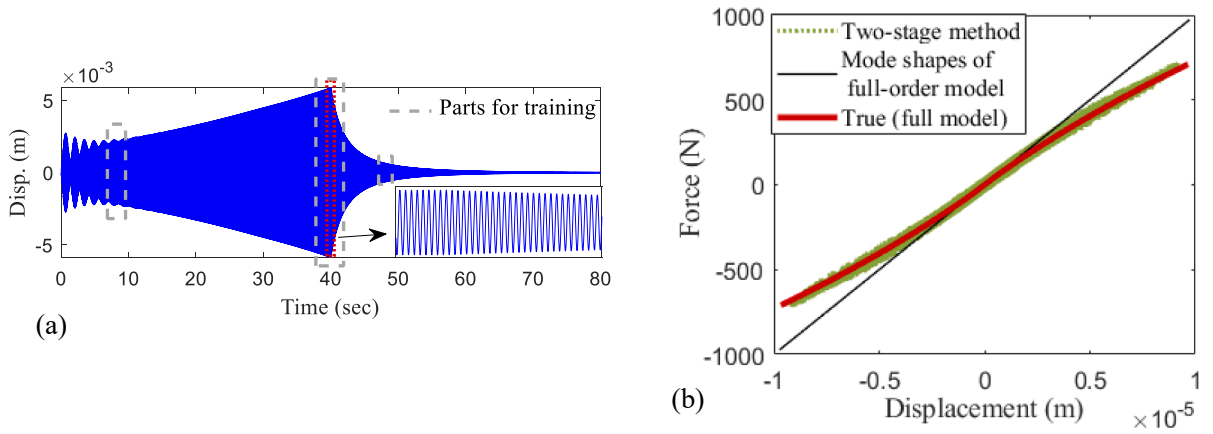


**Fig. 6.** Response of the beam under periodic excitation (a) Displacement response of the beam tip (point 12) (b) reconstructed force displacement response of an outer patch joint.

**Table 3**
Scenarios of using modal equations and couplings in the identification process (based on ROM4).

| Scenarios | Description |
|---|---|
| S1 | 1 modal equation of motion with no modal coupling in the nonlinear part |
| S2 | 1 modal equation of motion with modal coupling in the nonlinear part (10 modes) |
| S3 | 10 modal equations of motion with all 10 bending modes coupling in the nonlinear part |

configuration. Besides, the estimated parameters for the outer patches (elements 1 and 5) are close to the set true values. This would imply that the nonlinearity in the outer patches contributes more to the system response. Interestingly, the estimated values for the parameters of the middle patch (element 3) resulted to be negligible, suggesting that the middle patch can be simply assumed to be linear.

When the MSE values for each scenario are compared, the model with only one mode and no modal coupling has the highest error. However, when the modal couplings are considered in the model for S2, the error is significantly reduced. It is also discovered that including the modal equations for the higher modes in the S3 results in a lower fitting error, but the error is comparable to when only one mode is considered with modal couplings (S2). This could be justified because the model is only excited near its first natural frequency, and the contribution of the first mode to the system response is much greater than the contributions of the other higher modes.

**Table 4**
Estimated parameters of Iwan model using different reduced systems based on ROM4 as per Table 3.

| Model | Nonlinear element | Estimated | | | | MSE |
|---|---|---|---|---|---|---|
| | | $f_y$ | $k_t$ | $\chi$ | $\beta$ | |
| True | All | 2000 | 1.00E + 08 | −0.5 | 0.1 | – |
| S1 | 1 | 1696.2871 | 1.00E + 08 | −0.4920015 | 0.1380483 | 0.37 |
| | 2 | 1005.4768 | 1.00E + 08 | −0.1803442 | 0.2467595 | |
| | 3 | 34.73 | 1.00E + 08 | −0.01 | 0.01 | |
| | 4 | 904.0644 | 1.00E + 08 | −0.1208816 | 0.2326448 | |
| | 5 | 1781.5424 | 1.00E + 08 | −0.5545744 | 0.2217896 | |
| S2 | 1 | 1945.4488 | 1.00E + 08 | −0.4543532 | 3.999E-09 | 0.007 |
| | 2 | 2383.3059 | 1.00E + 08 | −0.5616309 | 0.4474936 | |
| | 3 | 3473 | 1.00E + 08 | −4.159E-10 | 1 | |
| | 4 | 1204.999 | 1.00E + 08 | −0.6558938 | 2.575E-06 | |
| | 5 | 2191.0106 | 1.00E + 08 | −0.493441 | 0.1727594 | |
| S3 | 1 | 1981.0566 | 1.00E + 08 | −0.4934634 | 1.54E-08 | 0.006 |
| | 2 | 2087.949 | 1.00E + 08 | −0.4560434 | 0.1107443 | |
| | 3 | 8.14E-11 | 1.00E + 08 | −0.9997673 | 7.95E-11 | |
| | 4 | 2040.18 | 1.00E + 08 | −0.3717837 | 0.0905626 | |
| | 5 | 1924.6249 | 1.00E + 08 | −0.5224398 | 3.23E-10 | |

Furthermore, the accuracy of the identified models is shown in Fig. 7 in terms of the modal nonlinear force–displacement relationship. For this purpose, the response of system with true and identified models (reported in Table 4) is calculated under the same harmonic sweep sine force with amplitude 40 N and frequency sweeping back from 76.5 to 78 Hz at the point 3 (see Fig. 3) from which the nonlinear part ($f_{nl}$) of the Eq. (10) is extracted. From Fig. 7, it is observed that the identified model based on S1 is not accurately reproducing the nonlinear force. However, identified models based on S2 and S3 are following the force–displacement maps for the different modes. These results suggest that it is beneficial to consider the modal couplings of higher modes in the identification process even when a simple modal equation is used. Besides, it can be seen that using only one modal equation (S2) would be sufficient for the identification of the nonlinear structure in this study and will indeed reduce the computational cost of the identification process.

To further assess the accuracy of the identified models using the abovementioned scenarios, a Monte Carlo simulation is conducted here. Similar to Section 3.2, zero-crossing method [5] is used to calculate the instantaneous amplitudes, frequencies and damping ratios from resonance decay responses. A variation of parameters for the Iwan model is considered based on normal distribution and structural response is calculated for each parameter set. This shows the sensitivity of the dynamic response to the variation of parameters in the nonlinear model used. A normal distribution is considered for all parameters. The true parameters are used as mean values (Table 4) with a standard deviation of 5 percent of the mean values. The distribution of the parameters can be seen in Fig. 8a. Similar modal displacement of 0.004 m at the beam tip (point 12) for the first mode is considered to initialise the simulations of the models in Table 3. The grey shade in Fig. 8 shows the results of the simulations based on 100 samples randomly generated. The responses of the identified models (S1-3) are also overlaid in Fig. 8. It can be seen that they all are within the response bounds of the uncertain true system, and this shows that they might be used to identify and characterise the form of nonlinearity in the structure and predict the amplitude dependent responses of the system. Therefore, it seems to indicate the promising scenario of only using one of the modal equations in the model selection process as it is more computationally efficient. Afterwards, the accuracy of estimated parameters can be enhanced by considering a model with nonlinear modal coupling.

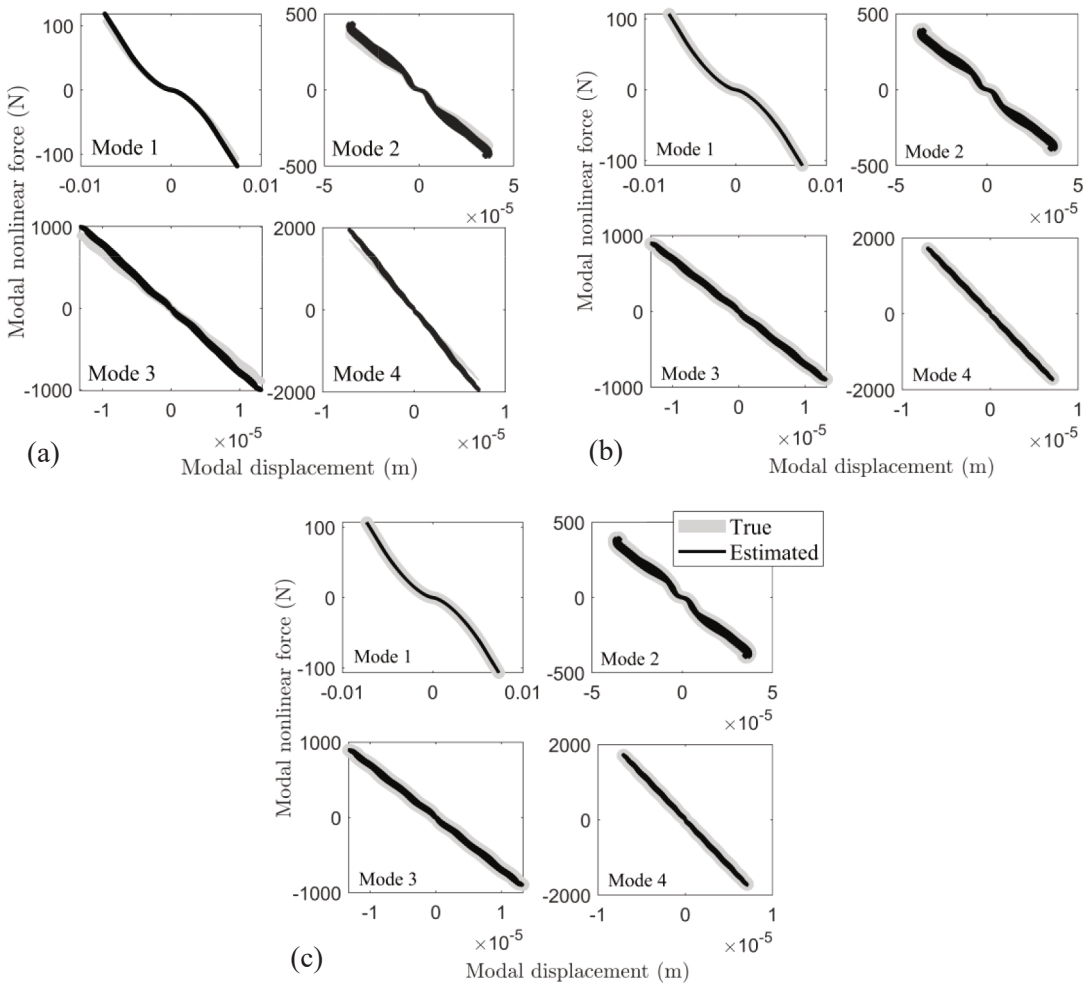


**Fig. 7.** Modal nonlinear force of the identified models (a) S1, (b) S2, (c) S3.

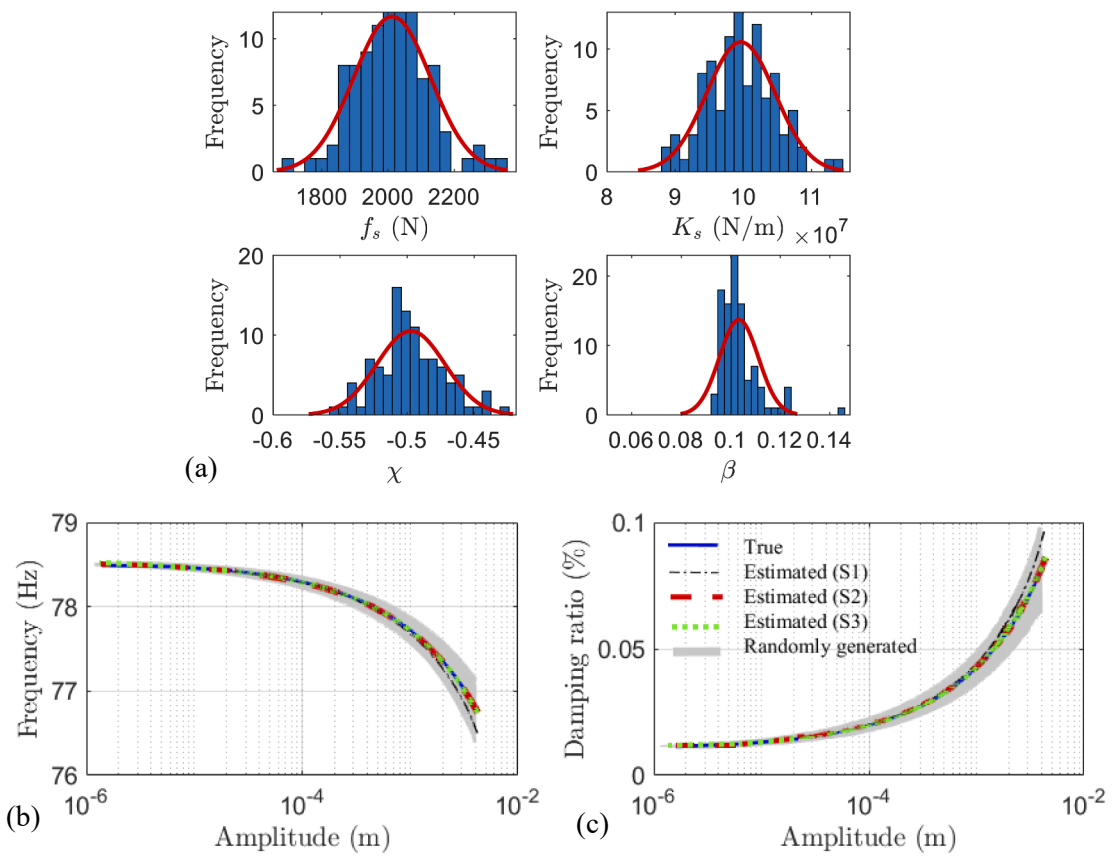


**Fig. 8.** Amplitude dependent response recorded at beam tip (point 12) using the identified models (a) histogram with the distribution of nonlinear model parameters, (b) instantaneous frequency, (c) instantaneous damping ratio.

### *3.4. Nonlinear model selection*

In this section, the nonlinear model selection is carried out based on the approaches and results introduced in Sections 2.3 and 3.3 respectively, and therefore only the scenario S2 is considered (i.e., only the equation of motion for a single mode with nonlinear modal coupling). That is, here we assume that the nonlinear model is unknown and use the presented approach to characterise and quantify the model. It should be noted that the selected portion of responses shown in Fig. 6 is used as training data and the stopping criteria described in Section 2.3 for model selection algorithm are set $\varepsilon_1 = \varepsilon_2 = 1 \times 10^{-5}$. The model selection algorithm is initialised using the values for the underlying linear system which are assumed to be known. We also assume that the nonlinear model for all 5 patches is

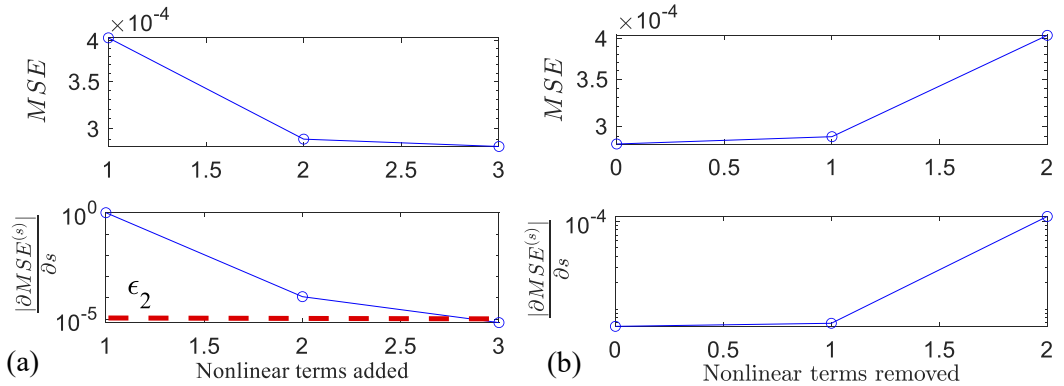


**Fig. 9.** Nonlinear model selection of the virtual experiment (a) Forward model selection convergence (b) Backward model selection convergence.

similar (but unknown). Fig. 9 shows the progression of nonlinear model selection using FB algorithm introduced in Section 2.3. It can be observed that three terms are added from library to the five nonlinear elements built in the finite element model. This model includes the combination of following terms in Table 1: {45, 22, 23}|q|q̇|q|q̇. Backward elimination algorithm removes two out of three terms in the nonlinear model, correctly identifying the Iwan model which is the remaining term (number 45 in Table 1). The estimated parameters for the selected model are identical to what is reported in Table 4 for S2 case.

Fig. 10 presents the comparison of time series obtained at the beam tip for the true (ROM4 + true nonlinear model) and identified model. As it was reported above, the training data for the model identification are only the input force and responses of the selected parts in Fig. 6. For validation, a sweep sine excitation force is applied at the point 3 with force amplitude 30 N and sweeping back frequency between 78 and 76.5 Hz. A good agreement can be observed for different amplitude levels of response between the true and identified model near mode 1 resonance according to Fig. 10a. Fig. 10b also presents the comparison of response between the true and identified model near mode 2 resonance for further validation of the discovered model. Here sweeping back frequency between 290 and 288 Hz is used with force amplitude 20 N. The fact that the discovered model are accurate approximations for mode 2 resonance is also clear from the time history comparison between the true and identified models.

## 4. Physical experiment

In this section, the proposed methodology is employed to identify and build a mathematical nonlinear model of local nonlinear elements for the experimentally tested LBRB structure using measurement data. The structure is first tested using a low-level force hammer test to retrieve the underlying linear dynamic properties i.e., natural frequencies, damping ratios and mode shapes. Based on these properties the underlying linear FE model is updated in Section 4.2. Then, harmonic forces are used to excite the structure in the nonlinear regime. The time-domain data obtained from harmonic test is used in Section 4.3 to discover the nonlinear model of the structure under study assuming that the locations of nonlinear elements are known. The discovered model is validated in Section 4.4 based on different time-domain data and also stepped-sine test.

### *4.1. The experimental setup and measurements*

The dimensions of the LBRB structure tested here are as reported in Section 3.1 for the numerical study. Fig. 11a shows the test configuration with a close up of the joint in the Fig. 11b.

The beam is made of stainless steel 304 and the connection includes M8 grade 12.9 steel bolts, M8 grade 5 5/16–24 UNF nuts and standard M8 washers. Before testing, each bolt was tightened first to 14 N.m (70% of the prescribed torque values), with the center bolt tightened first followed by the outer two bolts, and then all again tightened to 20 N.m (equivalent to pre-tension 11.58 KN) in the same order. Care was taken to ensure a gap between the vertical surfaces at the ends of the half-width extensions by separating the surfaces with cardstock (0.2 mm). This bolting procedure was recommended in [57] for best repeatability, which ensures reliable measurements.

To update the FE underlying linear model of the structure, a roving hammer test is first carried out based on the 12 measurement points shown in Fig. 3. The mode shapes for the first (81.055 Hz), second (281.64 Hz), third (509.47 Hz), and fourth (833.5 Hz) YZ-plane bending modes are estimated form the vibration data and shown in Fig. 11c. In addition, the mode shapes obtained from the updated linear model also presented in Fig. 11c. Section 4.2 describes the details of linear model updating.

For the purpose of nonlinear identification, the structure is excited harmonically at frequencies around the mode more likely to

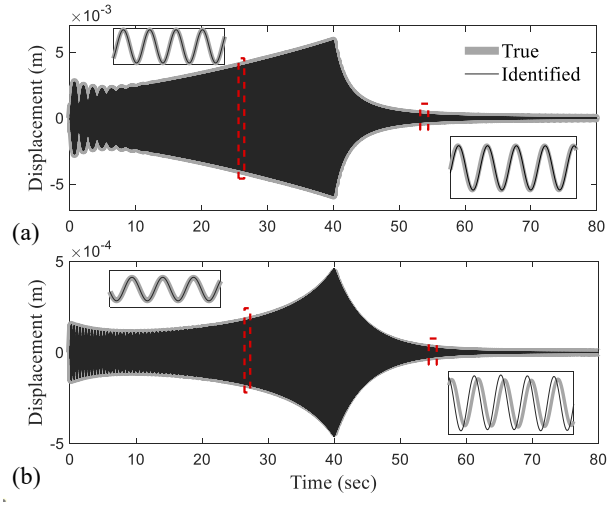


**Fig. 10.** Comparison of time series responses obtained from the point 12 for the true and identified models for virtual experiment structure (a) Mode 1 and (b) Mode 2.

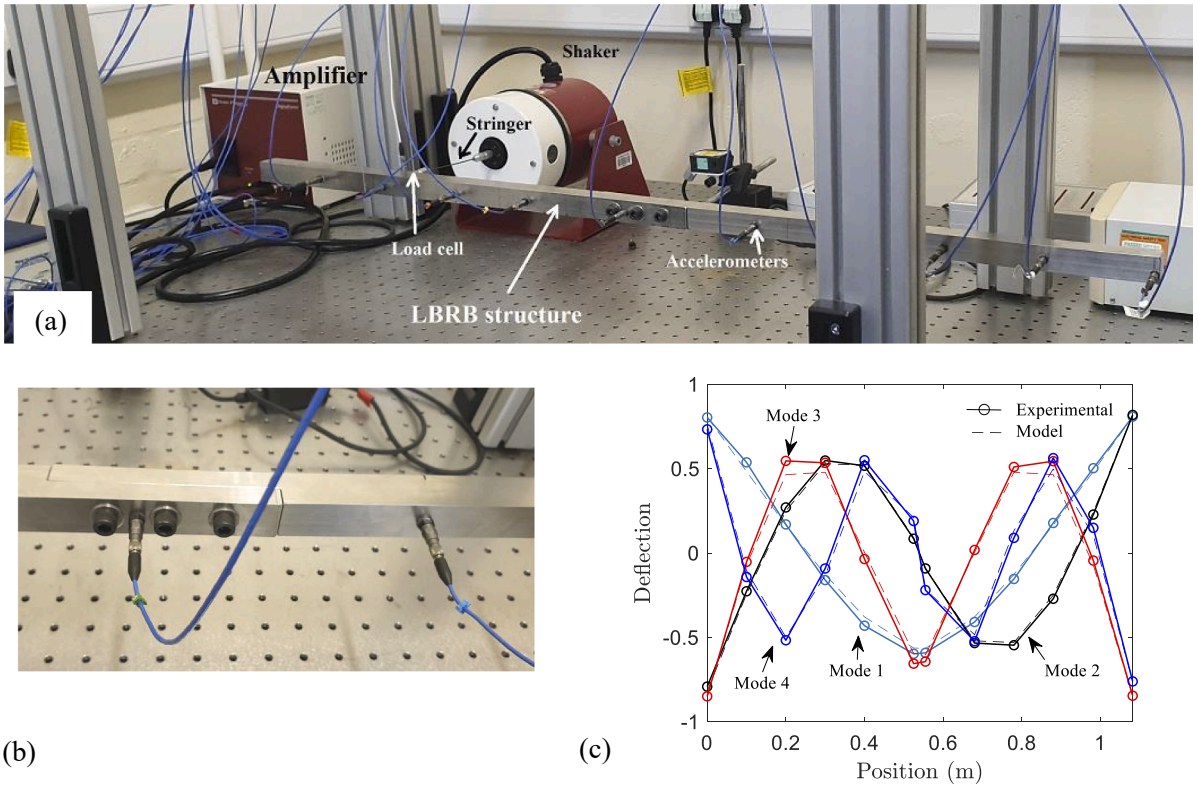


**Fig. 11.** The LBRB structure under test (a) test configuration, (b) close up of the joint, (c) first four bending linear mode shapes.

activate the nonlinear behaviour. The tests are conducted using the electrodynamic shaker (GV20-PA100E) attached to point 3 in the (Y) direction with a force sensor (PCB 208C02) to measure the shaker's driving force. As the beam was built to be symmetric, only seven piezoelectric accelerometers attached to the points 3, 6, and 8–12 are used in the tests. First and second bending modes are selected and excited using a sweep sine with frequency sweep nearby their natural frequency. The duration of time series are 21.875 s with sampling frequency of 25.6 kHz and the excitation sweeping frequencies are 78–83 and 278–281.5 Hz for the first and second mode respectively. For each mode, two different set of data are recorded for training and validation, which include free decay after reaching a large amplitude response around the resonance when the shaker is turned off. The forcing amplitude for training is 25 N, which near to the first mode resonance drops to 15.5 N (due to the shaker force drop-off -see Fig. 12a). The forcing amplitude for validation set is 27 N (which drops to 17.3 N due to the shaker force drop-off). The forcing amplitude is set to 20 N for the second resonance (see Fig. 12b).

In what follows, we analyse the time series data used as training sets. Fig. 12 presents the excitation force and the recorded

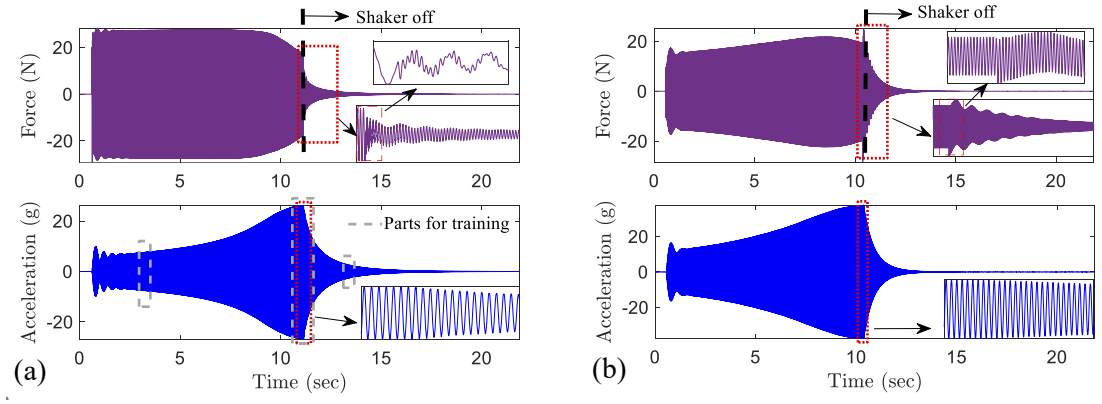


**Fig. 12.** Measured time histories of the input force and acceleration responses obtained from the point 12 under sweeping excitation (a) Mode1 and (b) Mode 2.

acceleration at the point 12 when exciting two first bending modes. Both time series show that the force acting on the structure does not drop to zero when the shaker is turned off. Which is due to the shaker-structure interaction. The shaker is intentionally attached near the node point of the first mode; therefore, it can be seen from Fig. 12a, that magnitude of measured force dropped rapidly and decays to zero in time. For mode 2 on the other hand, as the shaker is connected far form a nodal point, the shaker interaction is stronger resulting in a reactive force that reduces as the amplitude of vibration decays.

One significant benefit of the methodology discussed in this paper is that it decreases the negative effects of shaker-structure interactions on the identification process by directly using the input force and response time series in the identification process even when utilising data from the decaying part of the response. However, the nature of shaker-structure interaction is complex and investigating the effects of this type of phenomena on the proposed identification method still remains an open research topic that falls outside the scope of this paper.

In order to observe the contribution of different modes in the structural responses, we projected the measured responses into the linear modal coordinate using ten first bending mode shapes in the measurement direction (see Section 2.1, Eq. (9)). The cumulative energy for the first ten modal displacement responses is approximated using $E_u = \int_0^{t_f} |u(t)|^2 dt$ where $t_f$ is duration of response. The results of cumulative energy are plotted in Fig. 13 for both mode 1 and 2 responses shown in Fig. 12. It can be observed that the excited mode dominates the modal response for both data sets. This observation suggests that considering only the response of one mode might be enough for model discovery when the mode is excited. For the second mode, although the cumulative energy response of the main mode is one order of magnitude higher than the other modes, it might be effective to consider additional modes with higher contribution in the identification process. It is shown in Section 3.3 that considering modal couplings and the harmonics from higher modes can help with refined parameter estimation. Notice that this difference in terms of cumulative energy is likely due to the location of the shaker which is optimally placed for exciting the first mode (nearby a node) but is not for the second, and hence, changing the location of the shaker could improve the quality of the data should mode 2 be dominated by the nonlinear effects.

### 4.2. Linear model updating

The finite element model is first updated to ensure that it matches the first four bending modes in the measured direction along with their respective natural frequencies. For the linear model updating all the nonlinear elements are switched to linear springs, but otherwise, the finite element model is the same as that described in Section 3.1. An optimisation is carried out using a least-squares algorithm.

The target natural frequencies and mode shapes are those estimated from the low-amplitude vibration tests. The design variables are the Young's modulus (initially set to 200 GPa), and the stiffness of the (Y) direction and (Z) direction springs in all five joints. Due to the spatial symmetry of the bending modes, the Y and Z springs for joint 5 (refer Fig. 2c) are constrained to be the same as those for joint 1, and likewise those for joint 4 are constrained to be the same as those for joint 2. It should be noted that the constraint is applied only for the linear model updating. By reducing the number of unique design variables to seven, we create an overdetermined problem, which can be solved using least-squares optimisation. The variable space is normalised using logarithmic scale.

The parameters updated at the end of the optimisation problem are listed in Table 5, and the FE model natural frequencies are given in Table 6. The model mode shapes are compared with those of experiment in Fig. 11. There is an excellent agreement between the linear natural frequencies and mode shapes calculated from the model and those obtained from the experiment.

### 4.3. Nonlinear model updating

Now the proposed methodology is applied to identify the nonlinear models for the multiple nonlinear joints using data from the physical test structure. The identified linear model in the Section 4.2 is used to initialise the nonlinear model updating process. For this purpose, the values estimated for linear springs of the joints (see Fig. 2) are replaced in the finite element model and the damping

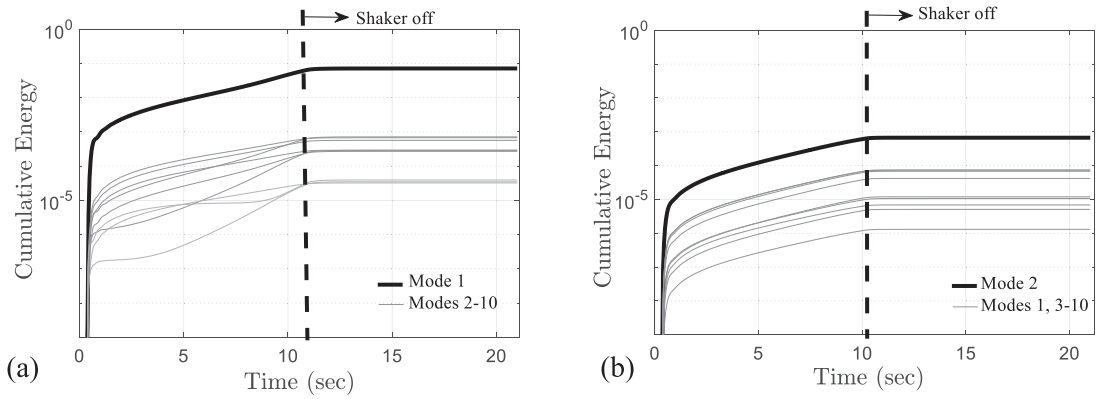


**Fig. 13.** Cumulative energy plots for the modal displacement responses (a) Mode 1 and (b) Mode 2.

**Table 5**
Updated linear parameters for the LBRB finite element model.

| Parameter | Value |
|---|---|
| Young's Modulus | 184.085 GPa |
| Joints 1 and 5: y-spring | $1.95676 \times 10^{9}$ Nm$^{-1}$ |
| Joints 1 and 5: z-spring | $1.70582 \times 10^{8}$ Nm$^{-1}$ |
| Joints 2 and 4: y-spring | $6.44018 \times 10^{9}$ Nm$^{-1}$ |
| Joints 2 and 4: z-spring | $9.57534 \times 10^{7}$ Nm$^{-1}$ |
| Joint 3: y-spring | $4.41949 \times 10^{11}$ Nm$^{-1}$ |
| Joint 3: z-spring | $1.44823 \times 10^{8}$ Nm$^{-1}$ |

**Table 6**
Comparison between model and experimental natural frequencies.

| Bending mode | Natural frequency (Hz) | | | Damping Ratio (%) |
|---|---|---|---|---|
| | Experimental | Numerical | Error (%) | Experimental |
| 1 | 81.055 | 81.068 | 0.017 | 0.1 |
| 2 | 281.64 | 281.83 | 0.068 | 0.07 |
| 3 | 509.47 | 509.34 | 0.023 | 0.085 |
| 4 | 833.49 | 832.97 | 0.062 | 0.2 |

matrix is created using proportional viscous damping based on the values reported in Table 6. It should be noted that the damping ratios for the higher modes are fixed at 0.1%.

The three selected portions from the training data for mode 1 (shown in Fig. 12a), which include forced and decaying parts of the responses, are used here for model selection and parameter estimation. Since it is presented in Fig. 13 that the response of first mode is dominant, therefore, approach S2 (see Section 3.3) is used within the optimisation problem defined in Eq. (13) which means only the modal equation for mode 1 is used with couplings up to 10 first bending modes in the nonlinear part. It should be noted that due to the configuration of the joints the expected nonlinear model form for all five joints is assumed similar, however, different parameter values can be estimated for each. The stopping criteria described in Section 2.3 for model selection algorithm are set $\varepsilon_1 = \varepsilon_2 = 1 \times 10^{-3}$. The value for stopping criteria depends on different parameters such as noise level of recorded data and the terms included in the library. The sensitivity of model selection to the stopping criteria is the topic of our future contribution. The results of the model selection progression using FB algorithm are shown in Fig. 14. It can be seen that four terms were selected for the nonlinear elements included in the model (terms: {45, 27, 7, 18} in Table 1). The addition of the fifth model causes the MSE value to rise, resulting in the algorithm to stop and deliver four terms. After running the backward elimination, one of the terms is removed resulting in a following combination of terms {45, 27, 18}: (1) 4-parameter Iwan model, (2) $p(1)|\dot{q}|\dot{q}$ and (3) $p(2)\ \mathrm{sign}(q)\sqrt{|q|}\dot{q}$. In the identified model, every term has a physical interpretation, that is, a physical parameterized model is achieved. For example, the first term selected which contributes to reducing the discrepancy between finite element model and physical system is Iwan model. This is one of the widely used models for simulating frictional behaviour. The other two selected models indicate that nonlinearities are both displacement and velocity dependent.

The estimated parameters for the selection model using FB algorithm are reported in Table 7. The very first observation is that joints 1 and 5 (and likewise joints 2 and 4) have similar ranges of estimated parameters, confirming symmetry of the jointed structure under study. Besides, the parameters for joint 3 have lower estimated values, specifically the parameters directly related to the force, which suggests that this joint have a negligible contribution in characterising the dynamics. Therefore, one might sufficiently assume only linear model for the middle joint.

The identified nonlinear model now needs to be tested through the validation step which is the topic of next section.

### 4.4. Model validation

In this section, the generalisation ability of the model identified for the structure in the physical experiment is studied. Firstly, a data set from a different sweep sine test is used for model validation by comparing the time series. Secondly, the results of a stepped sine test are considered to assess the generalizability of the discovered model for various levels of input excitation and frequency. Fig. 15a compares the displacement response of the updated nonlinear model against the displacement measured at point 3 under a sweep sine test with sweeping frequency between 78 and 80 Hz (near mode 1) and force amplitude of 27 N (drops to 17.3 N near resonance) which applied at point 3 on the structures. After sweeping up, the shaker is turned off in order to observe the decay response from resonance condition. It can be observed that from this figure that the identified parsimonious model captures most of the dynamics of the system. Three close ups are also included in the figure where the predictions are evaluated particularly for initial transient, nonlinear resonance and decaying responses. A satisfactory match in terms of amplitude can be observed for the initial transient response with a slight time shift likely due to accumulated simulation errors. The evidence suggests that the model discovered from data provides a good approximation for the part of the response near resonance, where the prediction is accurate in terms of amplitude and frequency. Furthermore, the predicted decaying part of the response is highly correlated with the response

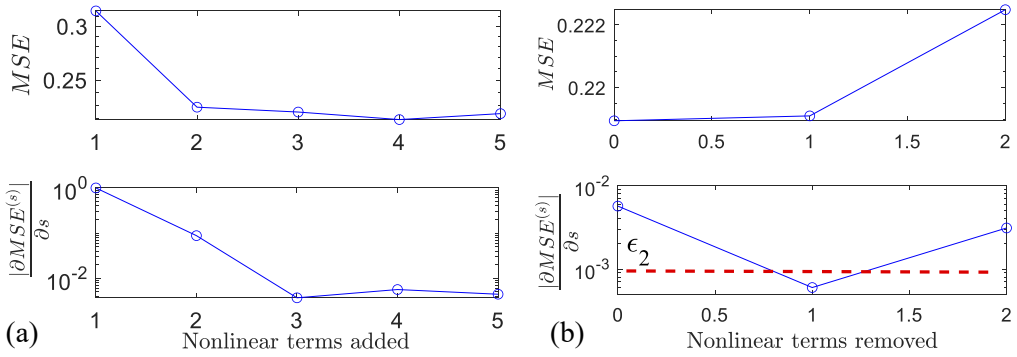


**Fig. 14.** Convergence of nonlinear model selection for the physical experiment (a) Forward (b) Backward.

**Table 7**
Estimated parameters of selected nonlinear model using FB algorithm.

| Joint No. | Selected terms | | | | | |
|---|---|---|---|---|---|---|
| | 45 (4-parameter Iwan model) | | | | 27 $p(1)$ | 18 $p(2)$ |
| | $f_y$ | $k_t$ | $\chi$ | $\beta$ | | |
| 1 | 3717.659486 | 170582317.2 | −0.5954 | 0.5065 | 5214215.175 | −0.4397 |
| 2 | 501219.7436 | 95753449.57 | −0.0003 | 0.9824 | 80.6606 | 1.2669 |
| 3 | 706.9696331 | 144823279.1 | −0.4142 | 0.4142 | 0 | 0 |
| 4 | 501,220 | 95753449.57 | −0.0003 | 0.9824 | 80.6606 | 1.2669 |
| 5 | 3710.776185 | 170582317.2 | −0.5954 | 0.507 | 5210394.778 | −0.4397 |

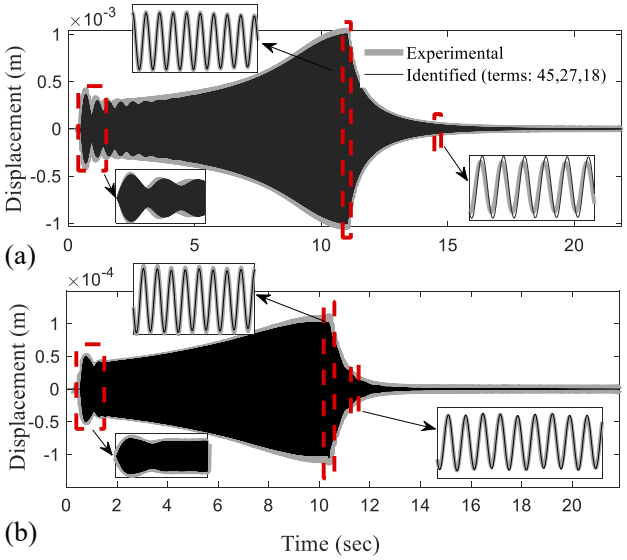


**Fig. 15.** Comparison of time series responses obtained from the point 12 for the true and identified models for physical experiment structure (a) Mode 1 and (b) Mode 2.

experimentally measured.

Similarly, the displacement response of the updated nonlinear model is compared against the actual displacement measured at point 12 on the structures under a sweep sine test with sweeping frequency between 278 and 281.5 Hz (near mode 2) and force amplitude of 20 N applied at point 3. A good agreement can be observed between the measured responses and responses from identified model. The identified model is able to accurately reproduce the time domain response near the second mode of vibration in three different regions: initial transient, nonlinear resonance and decaying responses.

Fig. 16 exhibits a comparison between the predicted acceleration frequency response curves for several excitation levels versus the

experimental measurements. The experimental steady-state acceleration response amplitude from stepped sine test is obtained and the maximum value of the last 5 cycles is plotted for each set of forcing amplitude and frequency. Similarly, the amplitude of steady-state acceleration for each set of forcing amplitude and frequency is obtained from simulation using numerical continuation [58]. In particular, the prediction accuracy of the identified model near the first resonance is shown in Fig. 16a based on the stepped sine responses for excitation levels F={0.25,2,5,8,15} N. It can be observed that the frequency shift is captured in different levels of excitation. The amplitude is also approximated with good accuracy except for two excitation levels F={2,5} N where the identified model overestimates the response amplitude especially at resonance.

The generalisation ability of identified model is also assessed near the second mode resonance in Fig. 12b. We can see a consistent match between the measured nonlinear frequency response curves obtained from stepped sine test for excitation levels F={0.25,1,2,4} N, and the ones simulated with the identified model. Overall, the identified model could reproduce the responses with a satisfactory agreement with the experimental measurements. Nevertheless, it is observed that for most of the excitation amplitudes for both modes, the identified model underestimates the damping provided by the whole joint model. It seems to overestimate the damping at larger amplitudes. It should be noted that the whole joint modelling strategy used in this study is a simple representation of the joint behaviour that helps to include its effects on the dynamic response of the structure. Therefore, there might be loss of local dynamics due to the unmodelled complex contact behaviour of the lap bolted joint since the contact area is large and many nodes are in contact. One might be interested to use the nonlinear model identified in this paper in another structure with a same joint configuration, however, extra care and further verification would be required, as some parameter tuning might be needed based on the pretension load of bolts and operational condition.

## 5. Conclusions

This work presented a methodology and its application for the structural identification of a nonlinear assembly with weak nonlinearities due to bolted joints. The proposed methodology is well suited for mechanical structures which primarily exhibit linear behaviour but contain active nonlinear elements that become significant at higher excitation levels. Nonlinear models for those active nonlinear elements are discovered using an optimisation-based approach which for the first time supports identifying simultaneously both stiffness and damping nonlinearities from measured data. This approach is based on the concept of nonlinear algebraic regression, which has been inspired by the idea of minimizing residuals of internal and external forces in numerical solvers of dynamical equations of motion.

One of the main contributions of this paper is that it scales up this identification methodology to be applicable for complex structures by employing a virtual sensing technique which lifts the necessity of direct measurement in the location of active nonlinear elements. This is achieved using a model reduction scheme which helps to initially reduce the full-order model into an efficient reduced-order model in the physical domain. Subsequently, the equations of motion of this reduced-order model are projected into the modal domain. The equations of motion in the modal domain are directly used to formulate an optimisation problem to select the nonlinear model and estimate its parameters. The benefit of using a model reduction in the physical domain is that it provides a low-dimensional model for quick simulations while preserving the dynamic characteristics of the full-order model. Additionally, it helps to discover the models of local nonlinear elements.

The methodology proposed in this paper automatically discovers nonlinear model for active nonlinear elements using forward–backward model selection algorithm that enables extending the dynamical equations of motion of the underlying linear system with nonlinear terms. A numerical example followed by an experimental validation demonstrate the application of the proposed structural identification method to discover the equations of motion while explicitly accounting for modal coupling introduced by nonlinearities.

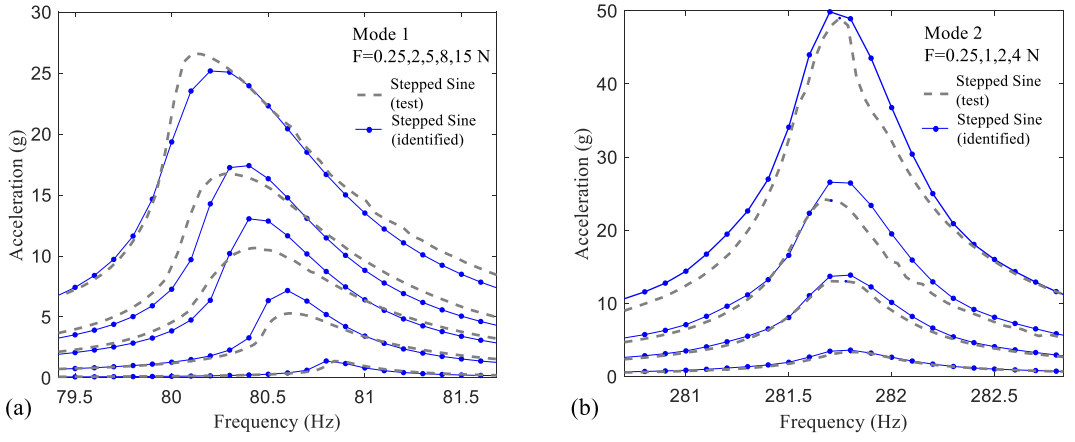


**Fig. 16.** Comparison of nonlinear frequency responses obtained from experimental test and identification (a) Mode1 and (b) Mode 2.

The results showed that parsimonious models can be selected from a comprehensive library of nonlinear terms for multiple joints included in the structure. Not only the proposed methodology allows physical interpretation through the selected model and parameters, but also the discovered nonlinear equations of motion offer a good generalisation. With the speed at which this data-driven identification methodology discovers and delivers the nonlinear models of locally unobserved nonlinear elements within the reduced-order systems of equations, it makes it ideal for updating nonlinear models of complex structures. Note that this approach has been developed to be performed in well-controlled laboratory conditions, hence, although in principle it could be applied to any full-scale structure the engineer would need to consider the ability to properly excite the required DOFs at the desired level of amplitude.

It is also important to highlight that the underlying linear modes of the structure under study are well separated and the nonlinearities are weak. The systems with strong nonlinearities typically induce sub- and super-harmonics and efficient identification of a reduced order model for them may need a multi-harmonic approach and amplitude-dependent reduction basis. Investigating the application of the proposed methodology for structures with close modes and strong modal interactions is a promising topic for future works. Also, the sensitivity of model selection to the stopping criteria can be followed in the future contributions. It is hoped that the methodology presented in this paper will inspire further improvements that will ultimately lead to a new industry standard for accurate and efficient structural identification of nonlinear assemblies.

## CRediT authorship contribution statement

**S. Safari:** Conceptualization, Investigation, Software, Validation, Visualization, Writing – original draft, Writing – review & editing. **J.M. Londoño Monsalve:** Conceptualization, Methodology, Supervision, Visualization, Writing – review & editing.

## Declaration of Competing Interest

The authors declare that they have no known competing financial interests or personal relationships that could have appeared to influence the work reported in this paper.

## Data availability

Data will be made available on request.

## Acknowledgments

Mr Safari is support by the scholarship from the Faculty of Environment, Science and Economy, University of Exeter which is gratefully acknowledged.

## References

[1] C.M. Richards, R. Singh, Identification of multi-degree-of-freedom non-linear systems under random excitations by the “reverse path” spectral method, J. Sound Vib. 213 (4) (1998) 673–708.
[2] G. Kerschen, J.-C. Golinval, K. Worden, Theoretical and experimental identification of a non-linear beam, J. Sound Vib. 244 (4) (2001) 597–613.
[3] P. Muhamad, N.D. Sims, K. Worden, On the orthogonalised reverse path method for nonlinear system identification, J. Sound Vib. 331 (20) (2012) 4488–4503.
[4] J.P. Noël, S. Marchesiello, G. Kerschen, Subspace-based identification of a nonlinear spacecraft in the time and frequency domains, Mech. Syst. Sig. Process. 43 (1-2) (2014) 217–236.
[5] J.M. Londoño, S.A. Neild, J.E. Cooper, Identification of backbone curves of nonlinear systems from resonance decay responses, J. Sound Vib. 348 (2015) 224–238.
[6] J.M. Londoño, J.E. Cooper, S.A. Neild, Identification of systems containing nonlinear stiffnesses using backbone curves, Mech. Syst. Sig. Process. 84 (2017) 116–135.
[7] K.J. Moore, Characteristic nonlinear system identification: A data-driven approach for local nonlinear attachments, Mech. Syst. Sig. Process. 131 (2019) 335–347.
[8] A. Ben Abdessalem, N. Dervilis, D. Wagg, K. Worden, Model selection and parameter estimation in structural dynamics using approximate Bayesian computation, Mech. Syst. Sig. Process. 99 (2018) 306–325.
[9] J. Taghipour, H. Haddad Khodaparast, M.I. Friswell, H. Jalali, An Optimization-Based Framework for Nonlinear Model Selection and Identification, Vibration 2 (4) (2019) 311–331.
[10] M. Scheel, G. Kleyman, A. Tatar, M.R.W. Brake, S. Peter, J.-P. Noël, M.S. Allen, M. Krack, Experimental assessment of polynomial nonlinear state-space and nonlinear-mode models for near-resonant vibrations, Mech. Syst. Sig. Process. 143 (2020) 106796.
[11] L.P. Miguel, R.d.O. Teloli, S.d. Silva, Bayesian model identification through harmonic balance method for hysteresis prediction in bolted joints, Nonlinear Dyn. 107 (1) (2022) 77–98.
[12] S.I.Z. Estakhraji, M.S. Allen, Extension of the Harmonic Balance Method for dynamic systems with Iwan joints, Mech. Syst. Sig. Process. 166 (2022) 108434.
[13] J.P. Noël, G. Kerschen, Nonlinear system identification in structural dynamics: 10 more years of progress, Mech. Syst. Sig. Process. 83 (2017) 2–35, https://doi.org/10.1016/j.ymssp.2016.07.020.
[14] C. Stephan, H. Festjens, F. Renaud, J.-L. Dion, Poles tracking of weakly nonlinear structures using a Bayesian smoothing method, Mech. Syst. Sig. Process. 84 (2017) 136–151, https://doi.org/10.1016/j.ymssp.2015.05.028.
[15] N. Peyret, J.-L. Dion, G. Chevallier, A framework for backbone experimental tracking: piezoelectric actuators, stop-sine signal and Kalman filtering, Mech. Syst. Sig. Process. 78 (2016) 28–42, https://doi.org/10.1016/j.ymssp.2015.09.020.
[16] D.J. Ewins, B. Weekes, A. delli Carri, Modal testing for model validation of structures with discrete nonlinearities, Philosophical Transactions of the Royal Society A: Mathematical, Phys. Eng. Sci. 373 (2051) (2015) 20140410.
[17] V. Ondra, I.A. Sever, C.W. Schwingshackl, A method for detection and characterisation of structural non-linearities using the Hilbert transform and neural networks, Mech. Syst. Sig. Process. 83 (2017) 210–227, https://doi.org/10.1016/j.ymssp.2016.06.008.

[18] A. Koyuncu, E. Cigeroglu, H.N. Özgüven, Localization and identification of structural nonlinearities using cascaded optimization and neural networks, Mech. Syst. Sig. Process. 95 (2017) 219–238, https://doi.org/10.1016/j.ymssp.2017.03.030.
[19] S.F. Masri, T.K. Caughey, A Nonparametric Identification Technique for Nonlinear Dynamic Problems, J. Appl. Mech. 46 (1979) 433–447, https://doi.org/10.1115/1.3424568.
[20] A.C. Gondhalekar, E.P. Petrov, M. Imregun, Parameters Identification for Nonlinear Dynamic Systems Via Genetic Algorithm Optimization, J. Comput. Nonlinear Dyn. 4 (2009), https://doi.org/10.1115/1.3187213.
[21] H. Samandari, E. Cigeroglu, A receptance based method for the calculation of nonlinear normal modes of large ordered structures with distributed localized nonlinearities, Int. J. Non Linear Mech. 147 (2022), 104240, https://doi.org/10.1016/j.ijnonlinmec.2022.104240.
[22] K. Vlachas, K. Tatsis, K. Agathos, A.R. Brink, E. Chatzi, A local basis approximation approach for nonlinear parametric model order reduction, J. Sound Vib. 502 (2021) 116055.
[23] E. Ferhatoglu, E. Cigeroglu, H.N. Özgüven, A novel modal superposition method with response dependent nonlinear modes for periodic vibration analysis of large MDOF nonlinear systems, Mech. Syst. Sig. Process. 135 (2020) 106388.
[24] H. Festjens, G. Chevallier, J. Dion, A numerical tool for the design of assembled structures under dynamic loads, Int. J. Mech. Sci. 75 (2013) 170–177, https://doi.org/10.1016/j.ijmecsci.2013.06.013.
[25] J.H. Porter, N.N. Balaji, C.R. Little, M.R.W. Brake, A quantitative assessment of the model form error of friction models across different interface representations for jointed structures, Mech. Syst. Sig. Process. 163 (2022) 108163.
[26] N.N. Balaji, M.R.W. Brake, A quasi-static non-linear modal analysis procedure extending Rayleigh quotient stationarity for non-conservative dynamical systems, Comput. Struct. 230 (2020) 106184.
[27] N.N. Balaji, W. Chen, M.R.W. Brake, Traction-based multi-scale nonlinear dynamic modeling of bolted joints: Formulation, application, and trends in micro-scale interface evolution, Mech. Syst. Sig. Process. 139 (2020) 106615.
[28] N.N. Balaji, M.R.W. Brake, The surrogate system hypothesis for joint mechanics, Mech. Syst. Sig. Process. 126 (2019) 42–64.
[29] R. Lacayo, L. Pesaresi, J. Groß, D. Fochler, J. Armand, L. Salles, C. Schwingshackl, M. Allen, M. Brake, Nonlinear modeling of structures with bolted joints: a comparison of two approaches based on a time-domain and frequency-domain solver, Mech. Syst. Sig. Process. 114 (2019) 413–438.
[30] R.M. Lacayo, M.S. Allen, Updating structural models containing nonlinear Iwan joints using quasi-static modal analysis, Mech. Syst. Sig. Process. 118 (2019) 133–157.
[31] R. Tibshirani, Regression shrinkage and selection via the lasso: A retrospective, J R Stat Soc Series B Stat Methodol. 73 (2011). https://doi.org/10.1111/j.1467-9868.2011.00771.x.
[32] C. Van Damme, A. Madrid, M. Allen, J. Hollkamp, Simultaneous regression and selection in nonlinear modal model identification, Vibration 4 (1) (2021) 232–247.
[33] S. Safari, J.L. Monsalve, Benchmarking optimisation methods for model selection and parameter estimation of nonlinear systems, Vibration 4 (3) (2021) 648–665.
[34] R.J. Guyan, Reduction of stiffness and mass matrices, AIAA Journal. 3 (1965). https://doi.org/10.2514/3.2874.
[35] O'CALLAHAN, John C, System equivalent reduction expansion process, Proc. of the 7th Inter. Modal Analysis Conf. (1989).
[36] R.R. Craig, M.C.C. Bampton, Coupling of substructures for dynamic analyses, AIAA J. 6 (7) (1968) 1313–1319.
[37] M.I. Friswell, S.D. Garvey, J.E.T. Penny, Model reduction using dynamic and iterated IRS techniques, J. Sound Vib. 186 (2) (1995) 311–323.
[38] H. Festjens, G. Chevallier, J.L. Dion, Nonlinear model order reduction of jointed structures for dynamic analysis, J. Sound Vib. 333 (2014) 2100–2113, https://doi.org/10.1016/j.jsv.2013.11.039.
[39] J.C. Loiseau, S.L. Brunton, B.R. Noack, From the POD-galerkin method to sparse manifold models, Applications (2020), https://doi.org/10.1515/9783110499001-009.
[40] M. Cenedese, J. Axås, H. Yang, M. Eriten, G. Haller, Data-driven nonlinear model reduction to spectral submanifolds in mechanical systems, Philos. Trans. R. Soc. A Mathemat. Phys. Eng. Sci. 380 (2022), https://doi.org/10.1098/rsta.2021.0194.
[41] M. Cenedese, J. Axås, B. Bäuerlein, K. Avila, G. Haller, Data-driven modeling and prediction of non-linearizable dynamics via spectral submanifolds, Nat. Commun. 13 (2022), https://doi.org/10.1038/s41467-022-28518-y.
[42] T. Simpson, N. Dervilis, E. Chatzi, Machine Learning Approach to Model Order Reduction of Nonlinear Systems via Autoencoder and LSTM Networks, J. Eng. Mech. 147 (2021), https://doi.org/10.1061/(asce)em.1943-7889.0001971.
[43] S. Safari, J.M. Londono Monsalve, Nonlinear function selection and parameter estimation of structures with localised nonlinearities, part 1: Numerical analysis, in: Conference Proceedings of the Society for Experimental Mechanics Series, 2021. https://doi.org/10.1007/978-3-030-47626-7_23.
[44] S.A. Billings, Nonlinear system identification: NARMAX methods in the time, frequency, and spatio-temporal domains, 2013. https://doi.org/10.1002/9781118535561.
[45] S.L. Brunton, J.L. Proctor, J.N. Kutz, W. Bialek, Discovering governing equations from data by sparse identification of nonlinear dynamical systems, PNAS 113 (2016), https://doi.org/10.1073/pnas.1517384113.
[46] A. Carderera, S. Pokutta, C. Schütte, M. Weiser, CINDy: Conditional gradient-based Identification of Non-linear Dynamics – Noise-robust recovery, ArXiv Preprint. (2021).
[47] K. Champion, P. Zheng, A.Y. Aravkin, S.L. Brunton, J.N. Kutz, A unified sparse optimization framework to learn parsimonious physics-informed models from data, IEEE Access 8 (2020) 169259–169271.
[48] Z. Lai, C. Mylonas, S. Nagarajaiah, E. Chatzi, Structural identification with physics-informed neural ordinary differential equations, J. Sound Vib. 508 (2021) 116196.
[49] S. Safari, J.M. Londoño Monsalve, Direct optimisation based model selection and parameter estimation using time-domain data for identifying localised nonlinearities, J. Sound Vib. 501 (2021) 116056.
[50] A. Singh, K.J. Moore, Identification of multiple local nonlinear attachments using a single measurement case, J. Sound Vib. 513 (2021), 116410, https://doi.org/10.1016/j.jsv.2021.116410.
[51] B. Peeters, H. Van der Auweraer, P. Guillaume, J. Leuridan, The PolyMAX frequency-domain method: A new standard for modal parameter estimation? Shock Vib. 11 (3-4) (2004) 395–409.
[52] T.D. Burton, W. Rhee, On the reduction of nonlinear structural dynamics models, JVC/J. Vibrat. Control. 6 (4) (2000) 531–556.
[53] M. Géradin, D.J. Rixen, Mechanical Vibrations: Theory and Application to Structural Dynamics, John Wiley & Sons, 2014.
[54] R. Isermann, M. Münchhof, Identification of dynamic systems: An introduction with applications, 2011. https://doi.org/10.1007/978-3-540-78879-9.
[55] J.B.W. Webber, A bi-symmetric log transformation for wide-range data, Meas. Sci. Technol. 24 (2) (2013) 027001.
[56] H.M. Hilber, T.J.R. Hughes, R.L. Taylor, Improved numerical dissipation for time integration algorithms in structural dynamics, Earthq. Eng. Struct. Dyn. 5 (3) (1977) 283–292.
[57] M.R.W. Brake, C.W. Schwingshackl, P. Reuß, Observations of variability and repeatability in jointed structures, Mech. Syst. Sig. Process. 129 (2019) 282–307.
[58] M. Krack, J. Gross, Harmonic Balance for Nonlinear Vibration Problems, Springer International Publishing, Cham, 2019. https://doi.org/10.1007/978-3-030-14023-6.